Investigation of Quantum Liquid in Binary Bose-Einstein Condensate at Lower Dimension

Thesis submitted to in fulfilment of the requirements for the Degree of

DOCTOR OF PHILOSOPHY

By

Argha Debnath

Under the Supervision of

Dr. Ayan Khan

School Of Engeneering And Applied Sciences

Department Of Physics

Bennett University,

Greater Noida - 201 310, INDIA

June, 2022

DECLARATION

I, *Argha Debnath*, Enrollment No. E18SOE808, hereby declare that the research work presented in this thesis titled *"Investigation of Quantum Liquid in Binary Bose-Einstein Condensate at Lower Dimension"* submitted to the *Department of Physics*, *School of Engineering And Applied Sciences*, *Greater Noida, India*, in partial fulfillment of the requirement for the awards of the degree of Doctor of Philosophy is original and is result of the investigation carried out by me under the supervision of *Dr. Ayan Khan*. The work is free from plagiarism. I have checked the thesis through a Plagiarism detection software Turnitin approved by the university. This work has not been submitted in any part or full for any other degree or diploma of this or any other institution.

Date:

Argha Debnath
Department Of Physics
Bennett University,
Greater Noida - 201 310, INDIA

CERTIFICATE

This is to certify that thesis titled *"Investigation of Quantum Liquid in Binary Bose-Einstein Condensate at Lower Dimension"* being submitted by *Argha Debnath*, Enrollment No. E18SOE808, for the award of the degree of Doctor of Philosophy, in *Department of Physics*, *School of Engineering And Applied Sciences*, *Greater Noida, India*, is a result of his investigation under my supervision. He has fulfilled all the requirements for the submission of the thesis under Ph.D. ordinance of the Bennett University. The work presented in this thesis is original and has not been submitted for any other degree or diploma in this or any other institution. The research work has also been checked for plagiarism using Software Turnitin and verified by the Research Committee.

Dr. Ayan Khan
Department of Physics,
School of Engineering And Applied Sciences,
Bennett University,
Greater Noida, 201 310,
UP, INDIA

to

those who love me

Contents

List of Figures

Acknowledgement

There have been several amazing people behind this thesis whose help is beyond measure. The most credit goes to my advisor, Dr. Ayan Khan, he not only is responsible for outlining the problems in this thesis, getting the necessary funding, teaching me the physics behind our research area, but he even periodically came and helped with the calculations inside this thesis. I walked on the road he paved for me, sometimes he gave me a free ride too.

I like to thank other research advisory committe members, Prof. Krishna Thyagarajan, Dr. Poulomi Sadhukhan, Dr. Neelam Choudhary, for their insightful comments during my research. Not to mention the unwavering support I got from faculty members of the department of Physics in Bennett University. In lab, help of Mr. Munna Lal Sharma and Mr. Shailendra Srivastava is unforgetful.

My respect and gratitude goes to all the seniors. In particular, (soon to be) Dr. Manish, (already) Dr. Tushar and (still have to wait to be) Dr. Sumit. I like to thank especially Sumit for being such a considerate roommate and also making me a permanent passenger in the backseat of his scooty.

I also want to thank my parents for worrying about the only fact “Are they still paying you?” and not to mention the beloved relatives and neighbours live with them.

I like to convey my respect and love for the only best thing happened during my graduate and post graduate years, was to be befriended with Tuhin, Rathin and Arijit da. Now, it’s time to thank rest of my friends with whom I grew up with. All my happy memories are made by them so I am enlisting them in alphabetical order : Apu, Ayan, Chinmoy, Diganta, Gourav (Boro), Kalyan, Kumaresh, Malay, Sandipan, Siddhartha, Shuvo, Supriyo, Tubu. Please forgive me if I miss anyone.

It's time to remember two people I could not be with in their last days, Mesho and Sayan. They say, you learn a lot about life when you lose someone very close. I surely acknowledge this unwanted burden that I have to carry all the way.

Abstract

The study of Bose-Einstein condensation in lower dimensions is considered to have a prominent role in understanding the fundamentals of many-body physics as they can be treated theoretically with relative ease and can be verified experimentally. Very recently, observation of a liquid-like state in a Bose-Einstein condensed mixture has been reported along with theoretical prescription for its observation in lower dimension. This observation is unique and has serious ramification in our prevailing conception of the liquid state which has deep influence of Van der Waals theory. In explaining the self-bound nature of these state, quantum fluctuations and it's fine balance with mean-field interaction turns out to be playing a key role. Though the experiments are performed predominantly in three-dimension however, theoretical studies extend to the lower dimensions as well. This thesis will mainly focus on analytical results related to this self- bound state in quasi one-dimension environment. It explores few results starting from the family of cnoidal solutions to droplet solutions with smooth transitions between each other and with a modest discussion about supersolid phase in between.

Chapter 1

Introduction

Temperature plays a key role in a change of phase of a matter. Usually, atoms in gaseous phase will change into liquid phase if temperature is reduced. The effect of temperature reduction restricts the movement of the atoms gradually. Inter-atomic distances start to drop and consequently increase their density. Atoms at far apart feel an attraction towards each other due to dipole-dipole interaction. Shorter atomic distance brings atoms closer enough to realize another force but a short-range repulsive one stems from the Pauli's exclusion principle for electron. As stated in the van der Waals's model, the emergence of liquid is a result of balance between these two counteracting forces at higher density [1].

Getting into a liquid phase prevents atoms to exhibit their quantum effects macroscopically. To make the wave function of the atoms macroscopic, it is necessary to keep atoms away from making molecules among themselves. The dilute quantum gases seem to be a perfect fit having a density of atoms four to six orders less than the density of atoms in the air at room temperature [2]. It was predicted that under a critical temperature a significant portion of atoms will condense into zero momentum state. This quantum mechanical phase transition leads atoms to become Bose-Einstein condensate (BEC) for bosonic atoms [2]. In a BEC, extended inter-atomic distance is far off the interaction range and that makes van der Waals forces to be harmless against forming a liquid state [2, 3].

In zero momentum state, interaction energy dominates over the kinetic energy of the atoms. Atoms with large de-Broglie wavelength treat the interaction as a contact poten-

tial [3]. The fact that atoms are condensed into a single particle state in a BEC triggers mean-field (MF) approximation theory [2]. The MF approximation excludes atom-atom correlations. Inclusion of correlations create a leak of atoms in non-zero momentum states. The fact that the leak or depletion of atoms in higher states is of order of one percent of total atoms, was a reason to neglect beyond MF (BMF) effect.

Interaction between the atoms can be repulsive or attractive. In case of repulsive interaction, there is no restriction on particle numbers that participate in forming a BEC. However, it is not the case for attractive interaction. A critical number can be found which restricts the maximum particle number in a BEC otherwise, a collapse of BEC will be seen as aftermath. For this reason, having a bound state in BEC have been an obstacle until Petrov's proposed theory came in 2015 [4].

According to the theory, a self-bound state can be achieved with a presence of prominent BMF effect in the mixture of two BECs rather than one. It is theorized that the participation of two BECs will modify the interaction co-efficients related to MF and BMF effect into an effective one. It is found that if the effective MF (EMF) interaction can be tuned into attractive interaction, effective BMF (EBMF) interaction term will still give a repulsive contribution. A liquid-like state can be achieved when EMF and EBMF contributions balance each other.

We note that the research on quantum liquid is not only limited to binary BEC mixture. It is found that quantum droplet can also be created in dipolar BEC. The later one is the result of balance among the short-range repulsive interaction born from a two-body contact pseudo-potential or MF interaction, the repulsive BMF effect can be noted as a typical attribute from quantum fluctuation, and attractive long-rang dipolar interaction. However, the self-bound nature in binary BEC comes from the opposite nature of MF and BMF effects, where interplay of inter-species and intra-species interactions plays crucial role.

Not so long after, a group of experimentalists has observed the formation of liquid droplet like state in a BEC mixture of dissimilar spin states of ^{39}K [5, 6, 7, 8, 9]. Quantum droplet was also created in heteronuclear mixtures of ^{41}K-^{87}Rb [10, 11] and ^{23}Na-^{87}Rb [12]. Diplolar quantum gases are also found to be great candidates for creating quantum

droplet and so far, experiments have been performed on ^{164}Dy [13, 14, 15, 16, 17], ^{162}Dy [18], ^{166}Er [19].

The dynamics BEC is quite successfully captured via MF formalism developed by Gross and Pitaevskii and therefore the nonlinear Schrödinger equation (NLSE) associated with BEC dynamics is known as Gross-Pitaevskii (GP) equation [20, 21]. Since the first successful realization of the atomic BEC, numerous works in this unique quantum state have taken place [22, 23, 24] which has widened our understanding about this intriguing phase of matter. These newly found droplets are self-bound due to the interplay of repulsive and attractive forces. The origin of the attractive force can be modelled in the purview of standard MF theory whereas the repulsive force originates from the BMF correction [25, 26]. The underlying theory relies on the Lee-Huang-Yang's (LHY) correction to the MF GP equation [27].

In this thesis we start with describing the theory related to binary BEC in chap. 2. We briefly give a theoretical model to obtain extended GP (eGP) equation with the inclusion of first order LHY correction or BMF term. In three-dimension (3D), The resulting eGP turns out to be a cubic-quartic NLSE (CQNLSE). We start from the 3D CQNLSE described in Eq.(2.3) and summarize the mathematical prescription to yield a quasi one-dimensional (Q1D) equation of motion [28]. Our primary interest is to obtain analytical solutions for Q1D CQNLSE in a cigar shaped BEC. The systematic dimensional reduction mechanism is employed to reduce the 3+1 dimensional problem to a 1+1 dimensional problem. Using the prescription of Ref.[28] we reduce 3+1 dimensional CQNLSE described in Ref.[6] to a Q1D CQNLSE.

In chap. 3, we start with a generic CQNLSE in cnoidal traps. We obtain analytical solutions considering different cnoidal traps. We found that the type of interaction whether attractive or repulsive, provided by MF and BMF interaction strengths, are important for the solutions to exist. Stability analysis on solutions are performed at the end of the chapter.

After using cnoidal traps, we extend our analysis to periodic traps in chap. 4. A driving force is also included to stabilize the system. We have also analysed one-dimensional (1D) NLSE in a periodic potential including BMF interaction and a driving force. After

exploring static solutions, we move onto dynamical analysis. Dynamical analysis reveals strip phase with a region in density for which a bound solution can be found.

In chap. 5, we analyse Q1D CQNLSE in a homogeneous environment. We obtain analytic solution, that point out droplet formation. It turns out that, the obtained solutions are valid for a particular relationship between MF and BMF interaction strengths. We perform modulation instability analysis on the solution. Numerical calculations are performed to verify analytically obtained solution.

We finally analyse Q1D CQNLSE in inhomogeneous case in chap. 6. Different ratio between MF and BMF interaction strengths are taken with different size of the trap for numerical calculation. Soliton to droplet transition can be seen with trap modification. If the geometry of the confined potential is significantly larger than the droplet size, the stablization of the solution is not affected. However, the situation changes when the size of the confining potantial becomes comperable to the droplet size. Stronger HO trap is resposible for a crossover, from one bound state to another.

Chapter 2

Theoretical Model

Let us consider at $T = 0$, a uniform binary mixture of Bose gases with masses m_1 and m_2 is condensed in a trap (V_{trap}). They are interacting with intra-atomic $g_{11} = 4\pi a_{11}\hbar^2/m_1$, $g_{22} = 4\pi a_{22}\hbar^2/m_2$, and inter-atomic coupling constant $g_{12} = 2\pi a_{12}\hbar^2/m_r$, where $m_r = m_1 m_2/(m_1 + m_2)$ is the reduced mass [29]. For this particular case, we consider positive intra-species (a_{11}, a_{22}) and negative inter-species s-wave scattering length (a_{12}) . The number of particles in respective species can be written in normalized form such that $\int n_1 dr = N_1$ and $\int n_2 dr = N_2$, where n_1, n_2 are the number densities of the corresponding species which are expressed in atomic units, a_B^{-3} (a_B being the Bohr radius) . The mixture can be characterized with the total number density, $n = n_1 + n_2$ and total number of atoms, $N = N_1 + N_2$. The energy density functional for this mixture can be written as [25, 6]

$$\begin{aligned} \varepsilon &= \varepsilon_{\text{kin}} + \varepsilon_{\text{trap}} + \varepsilon_{\text{MF}} + \varepsilon_{\text{BMF}} \\ &= \frac{\hbar^2}{2m_1}|\nabla\sqrt{n_1}|^2 + \frac{\hbar^2}{2m_2}|\nabla\sqrt{n_2}|^2 + (n_1+n_2)V_{\text{trap}} + \frac{1}{2}g_{11}n_1^2 + \frac{1}{2}g_{22}n_2^2 + g_{12}n_1n_2 + \varepsilon_{\text{BMF}}, \end{aligned} \tag{2.1}$$

The kinetic, potential, MF and BMF contributions are expressed with ε_{kin}, $\varepsilon_{\text{trap}}$, ε_{MF} and ε_{BMF}, respectively. An additional term i.e. ε_{BMF} in eGP equation includes the effect of quantum fluctuations. It has different form and interaction type depending on the dimension of the mixture. For 3D case, the BMF term has a repulsive contribution, it includes

the renormalization correction [30] to the scattering amplitude within the second Born approximation and for homonuclear mixture it stands as [4, 29]

$$\varepsilon^{3D}_{\text{BMF}} = \frac{8m^{3/2}}{15\pi^2\hbar^3}\sum_{\pm}\left(g_{11}n_1 + g_{22}n_2 \pm \sqrt{\left(g_{11}n_1 - g_{22}n_2\right)^2 + 4g_{12}^2 n_1 n_2}\right)^{5/2}.$$

$\varepsilon^{3D}_{\text{BMF}}$ can be expressed for different masses as

$$\varepsilon^{3D}_{\text{BMF}} = \frac{8m_1^{3/2}g_{11}^{5/2}}{15\pi^2\hbar^3}\mathcal{R}\left(\frac{m_2}{m_1}, \frac{g_{12}^2}{g_{11}g_{22}}, \sqrt{\frac{g_{22}}{g_{11}}}\right)|\sqrt{n_1 n_2}|^{5/2}.$$

For a particular case, $N_1 = N_2 = N/2$, $m = m_1 = m_2$, $g_{11} = g_{22} = g_{12} = g = 4\pi a\hbar^2/m$, $\varepsilon_{\text{BMF}} = \frac{256\sqrt{\pi}\hbar^2}{15m}(na)^{5/2}$ [29].

Here, $\mathcal{R} > 0$ is a dimensionless function and for the case of equal masses, $m = m_1 = m_2$, it can be written as $\mathcal{R}(1, y, x) = \sum_{\pm}\left(1 + x \pm \sqrt{(1-x)^2 + 4xy}\right)^{5/2}/4\sqrt{2}$ [4, 29].

In this approach, the spin excitations are neglected [4]. It is also assumed that the two components have the identical spatial mode as $n_{i=1,2} = |\Psi|^2$ and in the density ratio such that $n_1/n_2 = \sqrt{g_{22}/g_{11}} = \eta$. The following quantities can be defined as $g = \sqrt{g_{11}g_{22}}$ and $\delta g = g_{12} + \sqrt{g_{11}g_{22}}$. As a result, the energy functional can be re-written as

$$\begin{aligned}\varepsilon &= \varepsilon_{\text{kin}} + \varepsilon_{\text{trap}} + \varepsilon_{\text{MF}} + \varepsilon_{\text{BMF}} \\ &= \frac{\hbar^2}{2m}n|\nabla\Psi|^2 + V_{\text{trap}}n|\Psi|^2 + \delta g\frac{\eta}{(1+\eta)^2}n^2|\Psi|^4 + \frac{8m^{3/2}}{15\pi^2\hbar^3}(n\eta g_{11})^{5/2}|\Psi|^5, \quad (2.2)\end{aligned}$$

This energy functional leads to the following 3D CQNLSE [6]

$$i\hbar\frac{\partial\Psi}{\partial t} = \left[\left(-\frac{\hbar^2}{2m}\nabla^2 + V_{\text{trap}}\right) + U|\Psi|^2 + U'|\Psi|^3\right]\Psi, \quad (2.3)$$

where, $U = 2\delta g\frac{\eta}{(1+\eta)^2}n$, $U' = \frac{4m^{3/2}}{3\pi^2\hbar^3}(\eta g_{11})^{5/2}n^{3/2}$. There are two types of nonlinearity in the Eq.(2.3), the usual cubic nonlinearity due to MF interaction and an additional quartic

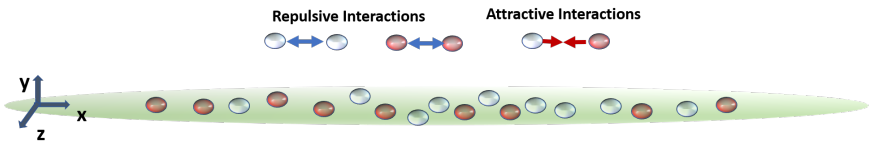

Figure 2.1: Schematic representation of two-component BEC in a Q1D confinement. The bluish and reddish spheres present atoms in the two different hyper-fine states. The intraspecies and interspecies interactions are repulsive and attractive respectively.

nonlinearity accounting the effect of BMF.

2.1 Treatment to Get Quasi-1D CQNLSE

Here, we consider homonuclear bosonic mixture similar to that of Ref.[5], where two hyperfine states of ^{39}K took part in the experiment, in a Q1D geometry. The situation can be visualized in Fig. 2.1 where the blueish and reddish spheres represent the different species of atoms (atoms in two hyperfine states) distributed in an effectively 1D cigar shaped trap. The intra-species interactions (g_{11} and g_{22}) are repulsive in nature and the inter-species interaction (g_{12} or g_{21}) is attractive. In binary BEC based on the strength of intra-species and inter-species interactions, it possible to define three distinct ground states. If g_{11}, g_{22} and g_{12} all are repulsive then one expects a transition between the miscible and the immiscible phase. However, the mixture can also collapse if the inter-species interaction is negative enough to counter the repulsive intra-species interactions. It can be shown that if $g_{12} > \sqrt{g_{11}g_{22}}$ then the mixture is in immiscible phase, if $-\sqrt{g_{11}g_{22}} < g_{12} < \sqrt{g_{11}g_{22}}$ then the condensate is in miscible phase and when $-\sqrt{g_{11}g_{22}} > g_{12}$ then the condensate collapses.

Now, in the miscible phase, but close to the collapse point i.e. $g_{12} > -\sqrt{g_{11}g_{22}}$, the attractive inter-species interactions overwhelms the repulsive interactions on each condensate. Close to the MF instability boundary i.e. $\delta g < 0$, $\varepsilon^{3D}_{\rm BMF}$ contibutes an imaginary term when negative sign in the sum in $\mathcal{R}$ is considered. It also leads to imaginary sound velocity. To avoid this ill effect created by the imaginary contribution, it is approximated that

$|\delta g| << g$ i.e. instability is very weak. Close to instability boundary, imaginary contribution is avoided by setting $|\delta g| \sim 0$ just for BMF term.

It is possible to describe the system with a single component effective GP equation [25] by neglecting the spin excitations. This criterion can be full filled by considering the two components occupy the same spatial mode [25]. The resulting one component equation of motion can be defined as [5],

$$i\hbar\frac{\partial\Psi}{\partial t} = \left[\left(-\frac{\hbar^2}{2m}\nabla^2 + V_{\text{trap}}\right) + U_{\text{sym}}|\Psi|^2 + U'_{\text{sym}}|\Psi|^3\right]\Psi, \tag{2.4}$$

where, $g_{\text{sym}} = g_{11} = g_{22}$, $\eta = 1$, $U_{\text{sym}} = \delta g n/2$ and $U'_{\text{sym}} = \frac{4m^{3/2}}{3\pi^2\hbar^3}g_{\text{sym}}^{5/2}n^{3/2}$ and m being the mass of the atoms. The equation is quite unique as there exist two types of nonlinearity, the usual cubic nonlinearity as well as an additional quartic nonlinearity. Here, it can be noted that NLSE with cubic and quintic nonlinearity is quite common in nonlinear optics [31] and BEC [32]. However, it is not the same for quartic nonlinearity. At this juncture, we also like to note that, in the early days of 21^{st} century, the possibility of droplet formation was explored via quintic nonlinearity as well [33]. Nevertheless, the repulsive term possessing quartic dependence manifests the BMF contribution, which is not well studied till date [34]. Therefore, we are primarily motivated to obtain an analytical solution for a NLSE which has both cubic and quartic nonlinearity.

Further, in Eq.(2.4), V_{trap} describes the external potential. It is possible to describe the external potential in terms of the transverse component ($V_T(y,z) = \frac{1}{2}m\omega_\perp^2(y^2+z^2)$) and longitudinal component ($V_L(x)$). Here, $\omega_\perp$ is the transverse trap frequency. The potential along the longitudinal direction is defined as, $V_L(x) = \frac{1}{2}m\omega_0^2x^2$ with ω_0 being the longitudinal trap frequency. In cigar-shaped BEC the transverse trapping frequency ($\omega_\perp$) is typically more than 10 times the longitudinal frequency (ω_0). It can be noted that in the early days of ultra-cold atom research, soliton trains were observed in 1D optical waveguide whose longitudinal (ω_x) and transverse trap frequencies ($\omega_\perp$) were set at $2\pi \times 50$Hz and $2\pi \times 710$Hz

respectively [35]. Since, the characteristic length scale happens to be $a_\perp = \sqrt{\frac{\hbar}{m\omega_\perp}}$, therefore in a Q1D geometry $a_x/a_\perp \sim \sqrt{10}$. Here, a_x is noted as $a_x = \sqrt{\frac{\hbar}{m\omega_0}}$ [36, 37]. This implies that the interaction energy of the atoms is much less than the kinetic energy in the transverse direction [37].

Consequently, it is possible to reduce Eq.(2.4) to an effective 1D equation. In order to perform the dimensional reduction, we have used the following ansatz similar to Refs.[28, 37],

$$\Psi(\mathbf{r},t) \;=\; \frac{1}{\sqrt{2\pi a_B}a_\perp}\psi\left(\frac{x}{a_\perp},\omega_\perp t\right)e^{\left(-i\omega_\perp t-\frac{y^2+z^2}{2a_\perp^2}\right)}. \tag{2.5}$$

Applying the ansatz from Eq.(2.5) in Eq.(2.4) we obtain the Q1D CQNLSE as noted below,

$$i\frac{\partial\psi(x,t)}{\partial t} = \left[-\frac{1}{2}\frac{\partial^2\psi(x,t)}{\partial x^2}+\frac{1}{2}Kx^2+\mathcal{G}_1|\psi(x,t)|^2+\mathcal{G}_2|\psi(x,t)|^3\right]\psi(x,t), \tag{2.6}$$

where, $\mathcal{G}_1 = \frac{\delta gnm}{4\pi a_B\hbar^2}$, $\mathcal{G}_2 = \frac{\sqrt{2}}{3}\frac{m^{3/2}n^{3/2}g_{\text{sym}}^{5/2}}{\pi^2 a_B^{3/2}a_\perp\hbar^5}$ and $K = \omega_0^2/\omega_\perp^2$.

Here, x and t are made dimensionless by $x \equiv x/a_\perp$ and $t \equiv \omega_\perp t$ [37]. The dimensionless notation of x and t will be followed from here onwards.

It is very important to note that BMF interaction co-efficient (previously defined as U', U'_{sym}, $\mathcal{G}_2$) is positive in 3D and also in Q1D but MF interaction co-efficient (previously defined as U, U_{sym}, $\mathcal{G}_1$) can be positive or negative in binary BEC. However, it is necessary to have a negative MF interaction co-efficient for achiving quantum droplet. At this point we are not attributing any sign to these two interaction co-efficients. We will analyze their natures while discussing the solutions of Q1D CQNLSE in different scenarios in following chapters. However, in lower dimension, specifically in 1D, the role is reversed i.e., EMF energy is repulsive while the BMF energy is attractive [38].

Chapter 3

Analysis Of A Generic CQNLSE

From the mathematical perspective, the described problem boils down to a nonlinear equation whose nonlinearity is not limited to the cubic term, but it also carries a quartic contribution in 3D and consequently in Q1D[6]. From our survey of literature, we realize that there exists a significant void in understanding the competition between cubic and quartic nonlinearity. We were only able to find out some discussion in Ref. [39, 40], where the authors have studied the existence of soliton in CQNLSE by using phase portrait analysis.

NLSE has drawn interest from diverse communities for the last several decades ranging from water waves to plasma. Formally, NLSE is the homogeneous second-order nonlinear differential equation and they admit different classes of the analytical solution. It is not difficult to map the NLSE to Jacobi Elliptic equation [28] which in turn allows us to use the 12 Jacobi elliptic functions as solutions. It must be noted that, the Jacobi elliptic functions can be derived from the amplitude function of Jacobi elliptic integrals [41, 42]. These solutions can be constant, periodic, or localized based on the parameter m as $0 \leq m \leq 1$. A broad class of the localized solutions are categorized as the solitons which are highly sought after in fiber optic communication system, as robust localized pulses with the ability to retain the shape over a large distance is highly amenable for long-distance communication [43].

In this chapter, we investigate the exsistance of cnoidal solution in Q1D system. Here, we will start from a trapped Q1D CQNLSE. We realize that the external trap plays a pivotal

role in stabilizing the solution in Q1D geometry. In the limiting case, the cnoidal wave solutions lead to the localized solution of bright solution and de-localized kink-antikink pair. The nonexistence of the sinusoidal mode in the current scheme is also revealed in our analysis.

3.1 CQNLSE In Cnoidal Trap

We realize that, understanding the interplay of cubic and quartic nonlinearity in a CQNLSE is the need of the hour. We consider a CQNLSE externally trapped in a Q1D geometry. Since, there exists a substantial void in the analytical description of the CQNLSE, we choose to start from the relatively simple Q1D geometry and provide necessary analytical insight. In this section, our main objective is to obtain cnoidal solutions from the Q1D CQNLSE therefore we set the external potential trap such a way that it allows the cnoidal solution to stabilize.

We realize that, the understanding with cubic and quartic nonlinearity is quite limited. Hence, we plan to revisit this unique problem in a more mathematical level. Thus, we take cnoidal trapping instead of harmonic and re-write Eq.(2.6) in more generic way. Nevertheless, we will explore the effect of K in Chap. 6.

$$\begin{aligned} i\frac{\partial\psi(x,t)}{\partial t} &= -\mathcal{A}\frac{\partial^2\psi(x,t)}{\partial x^2} + \mathcal{B}|\psi(x,t)|^2\psi(x,t) + \\ &\quad \mathcal{C}|\psi(x,t)|^3\psi(x,t) + \mathcal{D}(x)\psi(x,t) \end{aligned} \tag{3.1}$$

Here, $\mathcal{A}$, $\mathcal{B}$ and $\mathcal{C}$ are coefficients. In GP equation $\mathcal{A}$ is equivalent to $\hbar^2/2m$, where as in nonlinear fiber optics it defines the dispersion. $\mathcal{B}$ and $\mathcal{C}$ are the strength of the nonlinearities, where $\mathcal{B}$ can be connected to the short range two-body s-wave scattering and $\mathcal{C}$ defines BMF correction. $\mathcal{D}$ is the external potential. Here, we are interested in analyzing the static solutions and for that purpose we define, $\psi(x,t) = \phi(x)e^{-i\mu t}$. So, taking into account the

above considerations, Eq.(3.1) leads to,

$$\frac{d^2\phi(x)}{dx^2} + \alpha\phi(x) - \beta|\phi(x)|^2\phi(x) - \gamma|\phi(x)|^3\phi(x) \\ -\sigma(x)\phi(x) = 0, \tag{3.2}$$

where, $\alpha = \mu/\mathcal{A}$, $\beta = \mathcal{B}/\mathcal{A}$, $\gamma = \mathcal{C}/\mathcal{A}$ and $\sigma(x) = \mathcal{D}(x)/\mathcal{A}$. It must be noted that at this point, we are considering both the interactions (MF and BMF) as repulsive in nature. However, their exact characteristic can be understood after we obtain the exact solution.

3.2 Cnoidal Solutions

Since, cnoidal functions can lead to localized as well as sinusoidal modes based on the parameter value m, therefore, it is always beneficial if we can obtain a set of cnoidal solutions. We are primarily interested in finding the solutions in terms of the copolar trio, i.e., "cn", "sn" and "dn". Further, we know that the cnoidal functions at $m = 0$ and 1 can be written as, $\text{cn}(x, 0) = \cos x$, $\text{cn}(x, 1) = \text{sech}\, x$, $\text{sn}(x, 0) = \sin x$, $\text{sn}(x, 1) = \tanh x$, $\text{dn}(x, 0) = 1$ and $\text{dn}(x, 1) = \text{sech}\, x$. Moreover, the derivatives are defined as, $\frac{d}{dx}\text{sn}(x, m) = \text{cn}(x, m)\text{dn}(x, m)$, $\frac{d}{dx}\text{cn}(x, m) = -\text{sn}(x, m)\text{dn}(x, m)$ and $\frac{d}{dx}\text{dn}(x, m) = -m\,\text{sn}(x, m)\text{cn}(x, m)$. Hence, a careful evaluation of the above relations reveal that $\text{dn}(x, 1) = \text{cn}(x, 1)$, $\text{dn}(x, 0)$ is constant and derivative of $\text{dn}(x, 0)$ is zero. This allows us to concentrate only on "cn" and "sn" solutions without any loss of generality.

3.2.1 "cn" Solution

Let us define the first ansatz of the form $\phi(z) = A + B\,\text{cn}(z, m)$ where $z = \zeta x$ and ζ is the inverse of coherence length. We consider the external potential as $\sigma(z) = V_0\,\text{cn}^3(z, m)$. The external potential with strength V_0 actually plays a crucial role in stabilizing the system against the competing nonlinearities. The potential can be induced by means of an optical laser field. At this point, we are not explicating the physical nature of the potential however,

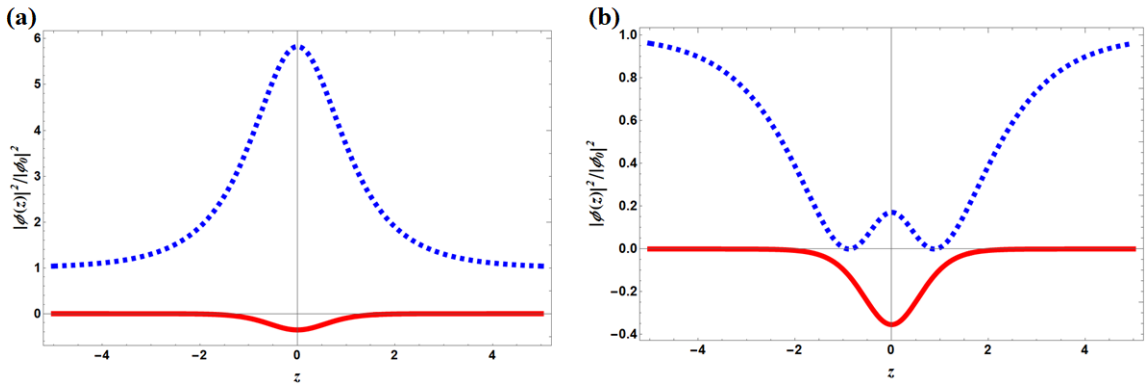

Figure 3.1: The dashed blue line in both the figures depicts two localized solutions representing Eq.(3.6). The solid red line describes the potential profile which is similar to the Pöschl-Teller potential. In (a) we observe bright soliton like structure however, (b) describes exotic w-soliton. Here, $\phi_0 = \beta/2\gamma$ and $V_0 = -\frac{\beta^3}{\gamma^2}$

.

after obtaining the solution we will definitely do so. Due to the change of variable, Eq.(3.2) modifies to

$$\zeta^2 \frac{d^2\phi(z)}{dz^2} + \alpha\phi(z) - \beta|\phi(z)|^2\phi(z) - \gamma|\phi(z)|^3\phi(z) - \sigma(z)\phi(z) = 0. \tag{3.3}$$

Applying the ansatz in Eq.(3.3) we obtain a set consistency condition,

$$\begin{aligned} &A^3\gamma + A^2\beta - \alpha = 0 \\ &4A^3\gamma + 3A^2\beta - \alpha - (2m-1)\zeta^2 = 0 \\ &4AB^3\gamma + B^3\beta + 2m\zeta^2 + AV_0 = 0, \\ &A = -\frac{\beta}{2\gamma},\ V_0 = -B^3\gamma. \end{aligned} \tag{3.4}$$

Solving Eq.(3.4) we obtain, $\zeta = \frac{B\sqrt{\beta}}{2\sqrt{m}}$ and $B = \pm\frac{\beta}{\sqrt{4-\frac{2}{m}\gamma}}$. Thus the strength of optical

potential can now be evaluated as, $V_0 = \mp\frac{\beta^3}{2\sqrt{2}(\frac{-1+2m}{m})^{3/2}\gamma^2}$. Hence, the solution is,

$$\phi(z) = -\frac{\beta}{2\gamma}\left(1 \mp \frac{\sqrt{2m}}{\sqrt{2m-1}}\text{cn}(z,m)\right). \tag{3.5}$$

However, the solution is acceptable if and only if, $\beta^3 - 8\alpha\gamma^2 = 0$. It must be noted that the MF interaction is repulsive otherwise, the coherence length will be complex which is totally undesirable. However, cnoidal solution does exist for repulsive as well as attractive BMF interaction. This counter intuitive situation is supported solely by the external potential. From Eq.(3.5) we observe that the solution does not exist for $m = 1/2$ and $m = 0$ leads to constant solution. Hence, a sinusoidal solution or "cos(x)" /"sin(x)" type of solution cannot be obtained in this framework. In summary, we can conclude that it is possible to obtain a localized solution corresponding to $m = 1$ however, the sinusoidal mode corresponding to $m = 0$ is absent.

3.2.2 Localized Solution

As per previous section, the cnoidal "cn" solution indicates the existence of localized modes as the solution exists for $m = 1$. Hence, from Eq.(3.5), the solution can be written as [34],

$$\phi(z) = -\frac{\beta}{2\gamma}\left(1 \mp \sqrt{2}\text{sech}(z)\right). \tag{3.6}$$

The external potential necessary to support the solution turns out to be $\sigma(z) = -\frac{\beta^3}{2\sqrt{2}\gamma^2}\text{sech}^3(z)$. In Fig. 3.1 we describe both solutions along with the potential profile. It must be noted that the Pöschl-Teller like potential (it must also be noted that, regular Pöschl-Teller type potential is $\propto$ sech$^2(z)$, whereas here the potential is $\propto$ sech$^3(z)$) actually allows to stabilize the localized solution as it is evident from the figures. Using $B = -\frac{\beta}{\sqrt{2}\gamma}$ we obtain bright soliton-like profile. However, contrary to the common perception, here we observe a non-zero background density of the bright soliton. As $z \to \pm\infty$, $|\phi(z)|^2 \to \beta^2/4\gamma^2$. Since two-body short-range interaction (β) and the BMF contribution (γ) are related to the scaled

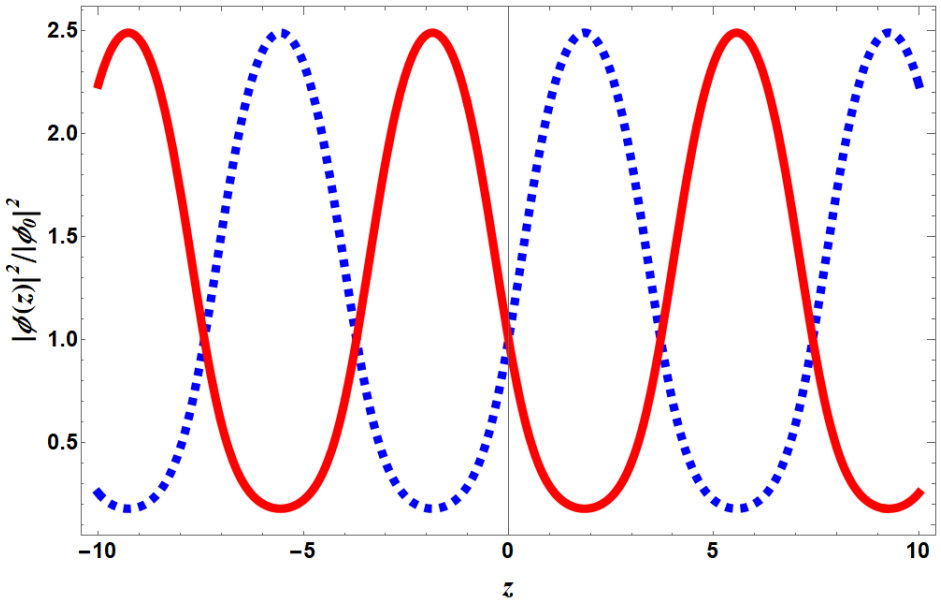

Figure 3.2: The figure depicts periodic behavior of "sn" solution for $m = 1/2$. The dashed blue line depicts $\phi_+(z)$ solution and the red solid line corresponds to the $\phi_-(z)$ solution from Eq.(3.7). Here, $|\phi_0|^2 = \beta^2/4\gamma^2$.

chemical potential (α) via $\beta^3 = 8\alpha\gamma^2$, therefore we can actually relate the background density in terms of the scaled chemical potential as noted in Ref. [38, 44]. Similarly, we also obtained w-soliton for $B = \frac{\beta}{\sqrt{2}\gamma}$ having a background density of $\beta^2/4\gamma^2$. The emergence of w-soliton is a manifestation of the competition between the interactions and its coupling with the trap. Similar observation has already been reported for strong coupling BEC [45]. The normalization of the system can be defined as $\int_{-\infty}^{\infty} |\phi(z)|^2 dz = N$ which leads to $N = \frac{(1+\pi/\sqrt{2})\beta^2}{\gamma^2}$ and $-\frac{(\pi/\sqrt{2}-1)\beta^2}{\gamma^2}$ corresponding to Fig. 3.1(a) and (b) respectively. However, as particle number is always positive therefore the w-soliton solution is not physically acceptable.

3.2.3 "sn" Solution

Next we use, $\phi(z) = A + B\,\mathrm{sn}(z, m)$ as ansatz and $\sigma(z) = V_0\,\mathrm{sn}^3(z, m)$. Applying the ansatz and the cnoidal potential in Eq.(3.2), we obtain, $A = -\beta/2\gamma$, $\alpha = \frac{\beta^3}{8\gamma^2}$, $\zeta = \frac{iB\sqrt{\beta}}{2\sqrt{m}}$,

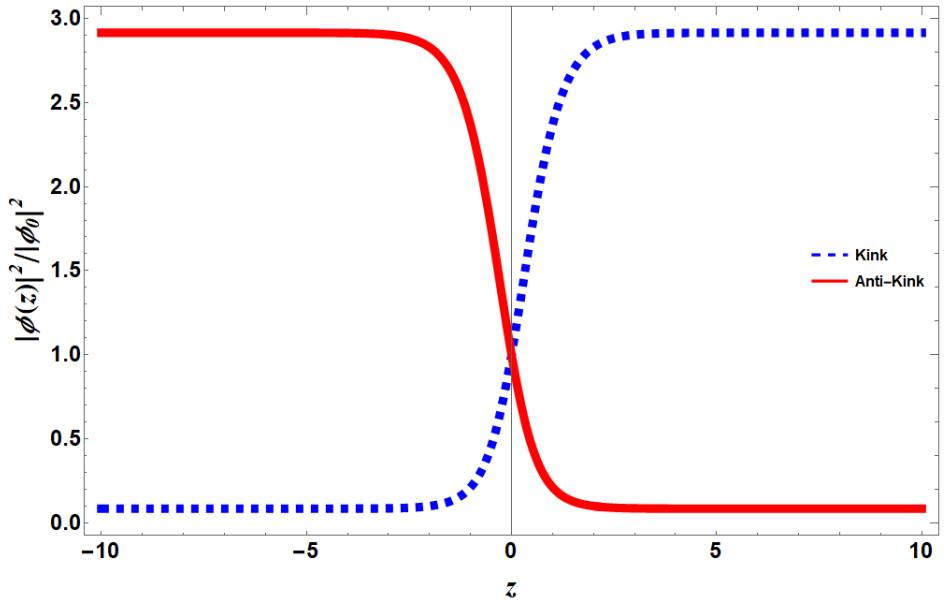

Figure 3.3: The figure depicts kink and anti-kink solution obtained from Eq.(3.7). Here, $|\phi_0|^2 = \beta^2/4\gamma^2$.

$B = \pm\frac{\beta\sqrt{m}}{2\sqrt{m+1}\gamma}$ and $V_0 = \frac{\beta^3 m^{3/2}}{8(m+1)^{3/2}\gamma^2}$. Here also we observe that for $m = 0$ the coherence length reduces to zero as $\zeta \to \infty$ which implies nonexistence of sinusoidal modes. However, the two-body scattering length must be negative or attractive otherwise the coherence length will be an imaginary quantity. Hence, the cnoidal wave solution reads,

$$\phi(z) \quad = \quad -\frac{\beta}{2\gamma}\left(1 \mp \frac{\sqrt{m}}{\sqrt{m+1}}\text{sn}(z,m)\right). \tag{3.7}$$

Contrary to the "cn" solution, we observe that "sn" solution yields nontrivial result for all values of m except $m = 0$ where the solution assimilates in the constant background. Fig. 3.2 describes the behavior of the two solutions for $m = 1/2$. The red solid line represents $1 - \frac{\sqrt{m}}{\sqrt{m+1}}\text{sn}(z,m)$ whereas the blue dashed line depicts $1 + \frac{\sqrt{m}}{\sqrt{m+1}}\text{sn}(z,m)$. We note these two solutions as $\phi_-(z)$ and $\phi_+(z)$ respectively. At $m = 1$ limit we yield kink-anti kink solution as described in Fig. 3.3. Kink and anti-kink solitons are common in the context of Sine-Gordon (SG) equation [46]. Albeit, the current nonlinear system is not same as the SG equation, nevertheless the solution boils down to the kink and anti-kink pair.

3.3 Stability

We have elaborated the existence of different types of solitonic solutions in the preceding section. Now, we will investigate the stability of the obtained soliton solutions in this section. Here, we plan to employ the well-known Vakhitov-Kolokolov (VK) criterion [47] for the localized solutions. The VK criterion has been widely used in determining the stability of the solutions of the NLSE, which predicts the parameter regime in the chemical potential where the soliton's amplitude can grow or decay exponentially [44, 45, 48]. The VK criterion states that a necessary stability condition is a positive slope [48] in the dependence of the number of atoms on the chemical potential. If, $\mathcal{N}_\mu = \partial N/\partial\mu > 0$, the solution is found to be stable and for $\mathcal{N}_\mu < 0$, the solution is unstable. One must note that the condition $\mathcal{N}_\mu = 0$ provides the instability threshold, $\mu = \mu_{th}$ [48, 49, 50].

It must be noted from Fig. 3.1 the asymptotic value of the solution leads to a flat bulk region contrary to the usual single soliton solution of NLSE [38]. Hence the number of atoms in the condensate, after subtracting the suitable background, can be defined as,

$$\begin{aligned} N &= \int_{-\infty}^{\infty}(|\phi|^2 - |\phi_0|^2)dz \\ &= \frac{(1+\pi/\sqrt{2})\beta^2}{\gamma^2} \quad \text{for bright soliton} \qquad (3.8) \\ &= -\frac{(\pi/\sqrt{2}-1)\beta^2}{\gamma^2} \quad \text{for } w\text{-soliton.} \qquad (3.9) \end{aligned}$$

Naturally, Eq.(3.9) is physically unacceptable hence we will concentrate on the stability of the bright soliton only. As α is the scaled chemical potential we can calculate $\mathcal{N}_\alpha = \frac{\partial N}{\partial \alpha} = \frac{8(1+\pi/\sqrt{2})}{\beta}$. Based on our previous discussion we know that β is always positive, hence $\mathcal{N}_\alpha$ is also positive. This enables us to conclude that the bright soliton is stable under the linear stability analysis.

To determine the stability criterion for kink soliton we need to analyze the effective potential $U(z)$ which can be computed from the fact $\zeta^2\frac{d^2\phi(z)}{dz^2} = -\frac{dU(z)}{d\phi}$. Here, $U(z) = \frac{\alpha}{2}|\phi(z)|^2 - \frac{\beta}{4}|\phi(z)|^4 - \frac{\gamma}{5}|\phi(z)|^5 - \frac{V_0}{2}\text{sech}^3(z)|\phi(z)|^2$. To analyze the stability of the kink it

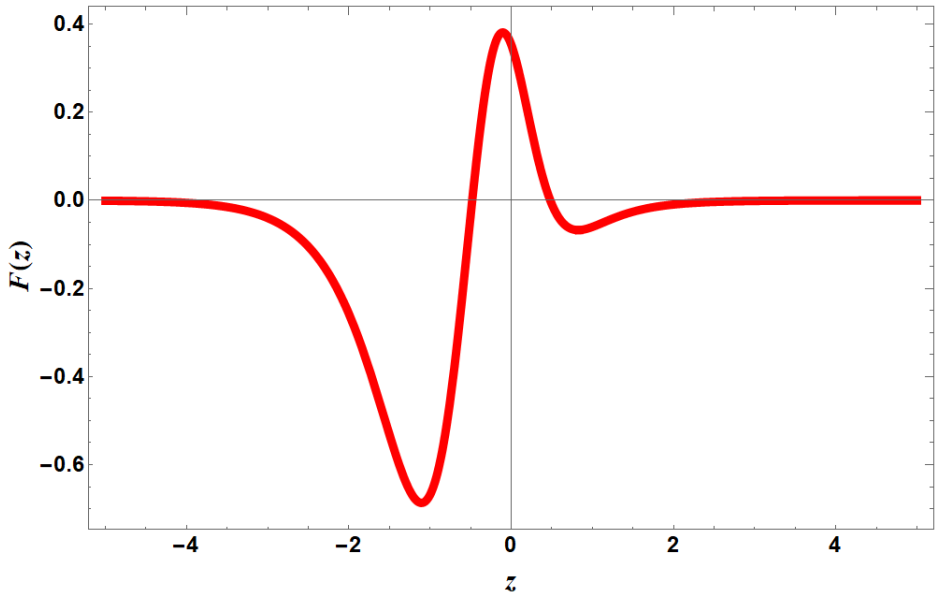

Figure 3.4: Variation of effective force $F(z)$. Here, we have chosen an arbitrary value of $\beta = -1$ and magnitude of γ is half the magnitude of β without loss of any generality.

is essential to calculate the effective force $F(z)$ where $F(z) = -dU(z)/dz$. One can now determine the stability of the kink by analyzing the zeros of $F(z)$ which can be noted from the Fig. 3.4. Let z_c corresponds to one such point, i.e., $F(z_c) = 0$. If $F(z) < 0$ for $z < z_c$ and $F(z) > 0$ for $z > z_c$ then $z = z_c$ is a stable equilibrium position for the kink [51]. Here, we find the zeroes of $F(z)$ lies at $z_1 = -0.47$ and $z_2 = 0.48$. Further, we see that, $F(z) < 0$ for $z < z_1$ and $F(z) > 0$ for $z > z_1$. Thus $z = z_1$ is a stable equilibrium position for the kink [51], whereas at $z > z_2$, $F(z) < 0$ and $F(z) > 0$ for $z < z_2$. Hence, we can conclude that the kink is in unstable equilibrium at $z = z_2$ [51]. In other words, the point z_c where $F(z)$ changes the sign correspond to the equilibrium positions with $\frac{dF(z)}{dz}|_{z=z_c} > 0$ being the stability criterion. Hence, the stability condition for the anti-kink can be noted as $\frac{dF(z)}{dz}|_{z=z_c} < 0$ [51].

3.4 Concluding Remarks

We analyze the possibility of obtaining cnoidal solutions in CQNLSE under the influence of an external trap. To obtain the cnoidal solutions, it is necessary to choose the external potential as a nonlinear cnoidal function. Our analysis reveals that, with cubic and quartic interaction it is unlikely that we can obtain any sinusoidal mode however localized (sech) and de-localized (tanh) modes can be obtained. A bright soliton-like solution is obtained under the influence of a Pöschl-Teller like potential (not exact Pöschl-Teller potential). Though we obtained a unique w-soliton, however it turns out that physically, the existence of this soliton is unlikely. An asymmetric step-like potential results delocalized solitons which are popularly known as kink and anti-kink. Further, we discuss the stability of these localized and de-localized solitons.

Chapter 4

Sinusoidal Modes In A Driven CQNLSE

Superfluidity and lattice order are mutually exclusive properties. However, there exists the theoretical proposition for the coexistence of such phases in nature which is popularly described as *supersolid*. Though solid ^4He is long considered as a prime candidate albeit decades of research unable to provide any unambiguous proof in that direction [52]. However, a set of recent experiments in ultra-cold atomic gases have actually exhibited the existence of such a counter-intuitive phase featuring antithetic properties [53, 54, 55, 56, 57]. This apparently contradictory phase of matter could yield deeper insights in understanding the superfluids and superconductors with far-reaching implications in the field of superconducting magnets and sensors, as well as efficient energy transport [58].

Chronologically, the emergence of droplet played the role of precursor in achieving the supersolid state in ultra-cold gases. The breakthrough in the alternative medium of cold-atom was realized when the signature of supersolid properties were noted in spin-orbit coupled BEC [53]. Later, supersolid properties were also observed in dipolar BEC. In these systems, the competition between short-range two-body scattering and long-range dipolar interaction plays detrimental role [55, 56, 57] in the emergence of supersolidity. The experiments were performed for dipolar alkali gases of ^{166}Er, ^{164}Dy and ^{162}Dy. The supersolid phase was observed in a well-defined parameter range in between the regular BEC and the droplet phase [57]. In a very recent experiment, the emergence and decay of supersolid state at finite temperature is also been noted [59].

The commonality between these two exotic phases arises from the fact that in both cases the BMF interaction plays a significant role in stabilizing the system. From the mathematical perspective, it boils down to a nonlinear equation where both odd and even exponent of nonlinearity plays a pivotal role, whence the origin of the even exponent arises from the LHY correction. It is interesting to note that, the even exponent is *two* for a strictly one-dimensional model whereas *four* in a Q1D model. Hence, the governing equation of motion in 1D system can be noted as quadratic-cubic nonlinear Schrödinger equation (QCNLSE) [38] and for Q1D system it turns out CQNLSE [60, 61]. It must be noted here that, the sinusoidal modes in a self-trapped QCNLSE have recently been discussed [62] apart from its localized counterpart [63]. On the contrary, in previous chapter we have seen that, in CQNLSE, nontrivial solutions do not exist for $m = 0$ where m is the moduli parameter of the cnoidal solutions [34]. Here we must remember that the cnoidal solutions lead to sinusoidal modes for $m = 0$. However, the localized solutions were demonstrated in chap. 3.

Nevertheless, the recent experimental developments motivate us to search for sinusoidal mode in Q1D setup. In this chapter, we show that it is possible to obtain trigonometric solution in a CQNLSE when trapped in bi-chromatic optical lattice (BOL) and subjected to a periodic driving force. The motivation to introduce BOL lies in the fact that it is generated by the superposition of two optical lattices (OL) [64] of different wavelengths and intensities. By tuning the power and the wavelength of the constituent laser beams, one can create a pure OL when required and vice-versa, allowing precise control over the shape of the trap profile [64]. The driving forces play the role of stabilization of the system. Here, we like to note that the stabilization process in a nonlinear system is a rudimentary subject with profound implications in diverse branches of science and technology. One of the fundamental aspects in this context is the theory of Lyapunov [65] where the stability of solutions near to a point of equilibrium were mainly focused. In recent times we have encountered proposition of noise-driven stabilization of nonlinear differential equations [66]. In this context, it must be noted that the externally driven, NLSE has been investigated in the context of a variety of physical processes such as Josephson junction, charge density

waves, twin-core optical fibres, plasma driven by rf field [67].

Here, the obtained periodic modes leave the signature of the existence of striped phase. Hence, our theoretical model promises a much simpler description to obtain a striped phase with potential supersolid properties. We extend our search of analytical solution for driven QCNLSE (DQCNLSE) as well. This allows us to comment on the analytical continuation of the nonlinear system from Q1D to 1D transition. In the later part, we concentrate on the coherent control of the driven CQNLSE (DCQNLSE) and investigate the spatio-temporal behavior of supercurrent as well as variation of energy density.

4.1 Static Solution

Off late, several investigations were dedicated towards a purely 1D system [38, 63] along with Q1D studies [34, 60, 61]. It is worth noting that 1D Bose gas does not support the formation of a condensate and therefore a quasi 1D geometry is widely used where the Bose gas is allowed to expand in an optical waveguide while enabling us to observe exotic structures like the bright soliton trains [35, 68]. Albeit, it is undeniable fact that the Bogoliubov theory correctly predicts the energy of a weakly interacting Bose gas by assuming the existence of condensate in one dimension [69, 70, 38].

At this juncture, it is also crucial to elaborate on the subtle difference between 1D and Q1D systems and dimensional crossover. In the crossover regime, a Q1D system assumes that $\sqrt{na^3} < 1$ where as for a 1D Bose gas, $\frac{1}{|\sqrt{n_{1D}a_{1D}}|} < 1$ [71]. n and a stand for the particle density and s-wave scattering length whereas n_{1D} and a_{1D} are the density and scattering length respectively in one dimension. It can be noted that $a_{1D} = 2\hbar^2 a/a_\perp^2 m$, with $a_\perp$ being the characteristic length scale of the trap and m being the mass of the particle [72]. The 1D counterpart of the density and scattering length can be noted as, $n_{1D} = nL^2$ and $a_{1D} = -L^2/2\pi a$ where L is the box length in which the system is confined. So, the dimensional crossover can be characterized by a parameter $\Sigma = naL^2$ [71]. $\Sigma \sim 1$ can be noted as the crossover and $\Sigma >> 1$ signifies strongly interacting 3D Bose gas while $\Sigma << 1$ defines a strongly interacting 1D Bose gas [4].

Our primary focus in this section is to determine the analytical solutions for time independent NLSE with BMF contribution in Q1D and 1D systems. This implies that we will hover around $\Sigma \geq 1$ (the exponent of nonlinearity from BMF contribution is 4) to $\Sigma \leq 1$ where the eGP equation is a QCNLSE. Hence, we start our investigation from a DCQNLSE and then extend the analysis to DQCNLSE (assuming the longitudinal trap frequency is very weak such that $K \to 0$). However, in Sec.4.2 we assume $K \neq 0$ and analyze the temporal behavior of the analytically obtained solution from DCQNLSE.

4.1.1 CQNLSE In Bi-Chromatic Lattice

We start from a CQNLSE in a BOL. It is already noted that the presence of two OLs of different frequency in same spatial dimension is favourable for the formation of supersolid where the effective lattice potential was described as a superlattice [53]. Additionally, we employ a periodic driving force as we realize that, to compete with the two-body MF interaction we require this contribution. It must be noted that in previous all experimental and theoretical descriptions (except Ref. [62]), we have seen that the two-body MF interaction is pitted against either dipolar or spin-orbit coupled interactions. In our analysis, the external force mimics the alternative force which competes with the regular two body interaction. Nevertheless, we also like to note that, the use of external driving force in ultracold atomic systems is nothing new. The suggestions regarding the transport of BEC atoms from a reservoir to the waveguide via a source/driving force can e found in Refs.[73, 74]. Here, the source term actually models the coupling of waveguide with a BEC reservoir. Very recently, we observe an analysis of QCNLSE using the source term [75]. Apart from these, GP equation in presence of external source and it's solution has already been studied quite extensively [67].

The knowledge of Eq.(2.6) allows us to write a generic time-dependent DCQNLSE as,

$$-\frac{1}{2}\frac{\partial^2\psi}{\partial x^2}+\left(V_2\sin\zeta x-V_1\sin^3\zeta x\right)\psi+g_1|\psi|^2\psi+g_2|\psi|^3\psi-i\frac{\partial\psi}{\partial t}=F'(x,t). \tag{4.1}$$

At this moment we focus on the static solution so that $\psi(x,t) = \phi(x)e^{-i\mu t}$, where μ is the chemical potential. The driving force is phase locked temporally with the solution and experiences sinusoidal modulation in the spatial dimension such that $F'(x,t) = Fe^{-i\mu t}\sin\zeta x$. Hence, the time independent DCQNLSE will read,

$$-\frac{1}{2}\frac{d^2\phi}{dx^2}+\left(V_2\sin\zeta x-V_1\sin^3\zeta x\right)\phi+g_1|\phi|^2\phi+g_2|\phi|^3\phi-\mu\phi=F\sin\zeta x. \tag{4.2}$$

Here, ζ is the inverse of coherence length, g_1 and g_2 are the strength of the cubic and quartic nonlinearities, respectively. V_1 and V_2 are potential depths of the periodic traps whose superimposition in the same spacial dimension creates a bi-chromatic landscape which can even be modulated to create a superlattice [53]. Frequencies of the two laser beams responsible in creating the BOL are commensurate. We can also express the BOL as, $V_{BOL} = \frac{V_1}{4}(3\sin(\zeta x) - \sin(3\zeta x)) - V_2\sin(\zeta x) = (\frac{3V_1}{4} + V_2)\sin(\zeta x) - \frac{V_1}{4}\sin(3\zeta x)$. Hence, it suggests that, apart from different amplitude, the wavenumber of one laser is required to be thrice of the second laser. In practice, the superlattice potential was created using two different laser beams associated with two different wavenumber albeit equal amplitude [53]. In a recent numerical study, the atoms were subjected to spin dependent periodic potential [76].

Further, F is the strength of the periodic driving force. We assume an ansatz solution of the form $\phi(x) = A + B\sin\zeta x$ and apply in Eq.(4.2). The rationale for choosing this specific type of ansatz is derived from the fact that the experimental observation of the density distribution of the supersolid phase is well fitted through a function of similar form

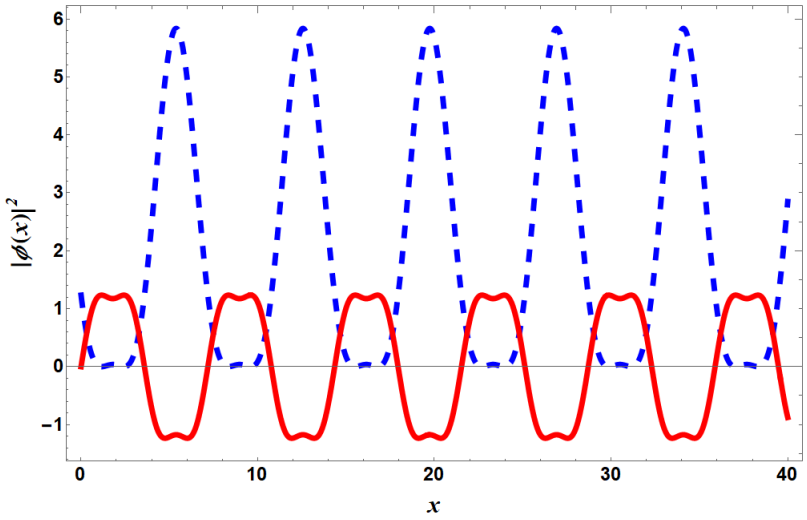

Figure 4.1: The density profile calculated from Eq.(4.8) is depicted here along with the bi-chromatic lattice potential. The blue dashed line describes the density variation ($|\phi(x)|^2$), where as the red solid line demonstrates the potential landscape (the bi-chromatic lattice or V_{BOL}) in the same spatial dimension. We have used arbitrary units for this plot such that, $V_1 = 1.0$, $V_2 = \frac{1}{3}\left(\frac{V_1}{g_2}\right)^{1/3}\frac{g_1^2}{g_2}$, $g_1 = 1.5$, $g_2 = 0.3$, $F = 0.5$.

[55]. Using this ansatz, we yield a set of consistency conditions.

$$A^2 g_1 + A^3 g_2 - \mu = 0 \tag{4.3}$$

$$6A^2 B g_1 + 8A^3 B g_2 + 2AV_2 + B\zeta^2 - 2B\mu - 2F = 0 \tag{4.4}$$

$$3ABg_1 + 6A^2 B g_2 + V_2 = 0 \tag{4.5}$$

$$B^3 g_1 + 4AB^3 g_2 - AV_1 = 0 \tag{4.6}$$

$$B^3 g_2 - V_1 = 0 \tag{4.7}$$

A careful analysis of the consistency conditions allows us to yield the exact analytical solution. First, we use Eq.(4.7) to determine B as a function of equation parameters, such as V_1 and g_2. This results $B = (\frac{V_1}{g_2})^{1/3}$. Using the fact $V_1 = g_2 B^3$, in Eq.(4.6) we immediately obtain $A = -g_1/3g_2$. Further, from Eq.(4.5) one can determine V_2 as a function of interaction strengths which yields $V_2 = \frac{Bg_1^2}{3g_2}$. All these information now allow us to explicate the

chemical potential (μ) as, $2g_1^3/27g_2^2$ deriving from Eq.(4.3). Lastly we obtain an expression for inverse coherence length or ζ as, $\zeta = \pm\left(\frac{2F}{B}\right)^{1/2}$ by using Eq.(4.4).

In Eq.(4.3-4.7), g_1, g_2, V_1 and F are equation parameters whereas A, B, μ, V_2 and ζ are the solution parameter. In actual experimental setup, V_2 can also be treated as known parameter so as ζ. However, we find here that it is not possible to treat V_2 and ζ as independent parameter rather they are coupled to the interaction strengths as well as driving force and V_1. Hence, from the experimental perspective, to obtain sinusoidal modes as described, we need to control V_2, the amplitude of the second laser, via precise control of the external magnetic field (through Feshbach resonance [77]) and amplitude of the first laser. Similarly, the coherence length is now coupled with the amplitude of the driving force as well as V_1 and g_2. Though our approach leads to these additional constrain condition however, it must not disregard the fact that the current formalism do suggest sinusoidal modes, which can lead to supersolid like phase, without taking into account dipolar or spin-orbit interactions.

Finally, we note that solution for Eq.(4.1) as,

$$\phi(x) = \phi_{Q1D}(x) = -\frac{g_1}{3g_2} + \left(\frac{V_1}{g_2}\right)^{1/3} \sin\zeta x. \tag{4.8}$$

These findings also suggests that $B \in \mathbb{R}$ to avoid the possibility of complex coherence length. In other words this also implies that the beyond mean-field interaction strength (g_2) is repulsive in nature along with the fact that $V_1 > 0$. However, it must be noted that there is no such restriction on the two-body interaction strength (g_1). Hence, the mean-field interaction strength can be attractive as well as repulsive. The driving force (F) must have the same direction as the displacement.

In Fig. 4.1 the spatial variation of density ($|\phi(x)|^2$) is depicted via blue dashed line. The red solid line describes the spatial variation of the BOL. From the figure, the existence of density wave is quite evident with density maxima coinciding with the potential minima.

It is now important to analyze the stability of these modes. It is well accepted that, for sinusoidal excitation in nonlinear Schrödinger-type equations, the stability can be examined

through the VK criterion [47, 48]. We define the number of atoms per lattice site as ($\mathcal{N}$). Here, we find that $\partial\mathcal{N}/\partial\mu = \mathcal{L}/g_1$ when we calculate the particle number in a unit cell of length $\mathcal{L}$. Hence, for the solution to be stable, g_1 must remain positive or repulsive in nature. It must be noted that in the experiments the stabilization mechanism of the periodic modes can be described by the contest between the short-range interaction with long-range dipolar interaction [55]. Similarly, in our model the repulsive short-range interaction is balanced by the driving force.

4.1.2 Quadratic-Cubic NLSE

On the contrary, to obtain an analytical solution for a driven 1D NLSE we need to switch off the BOL and an OL appears sufficient to support the solution. It is worth noting that in a QCNLSE, it is possible to obtain sinusoidal solution even without any lattice potential or external driving [62]. However, as a part of our systematic study of transition from Q1D to 1D geometry we intended to employ minimal change in the system. Through our survey, we realize that, a minor trap engineering by means of transforming a BOL to OL is sufficient to obtain the desired result.

Hence, we consider here the OL as $V_3 \sin^2(\zeta x)$. The equation of motion can be noted as,

$$-\frac{1}{2}\frac{d^2\phi}{dx^2} - \left(V_3 \sin^2 \zeta x + g_3|\phi| + g_1|\phi|^2 - \mu\right)\phi = F \sin \zeta x. \tag{4.9}$$

Following the same prescription as earlier in Eq.(4.9), we determine the wavefunction as $\phi(x) = \phi_{1D}(x) = -\frac{g_3}{2g_1} \pm \sqrt{\frac{V_3}{g_1}}\sin(\zeta x)$ and the chemical potential being $-\frac{g_3^2}{4g_1}$. The inverse coherence length remains same as previous such that, $\zeta = \pm\sqrt{\frac{2F}{B}}$. The density wave is preseted in Fig. 4.2 where the blue dashed line described the spatial density variation. The red solid line denoted the optical lattice potential. We like to note that $\phi_{1D} \neq \phi_{Q1D}$ and thus we lose the analytic continuation as observed till the previous section.

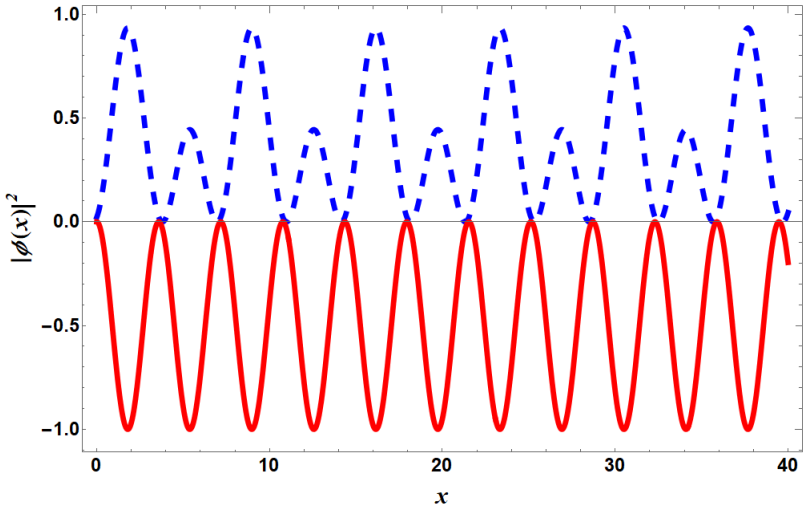

Figure 4.2: The density wave against the backdrop of the optical lattice potential for a DQCNLSE. The blue dashed line describes the density variation ($|\phi(x)|^2$), whereas the red solid line demonstrates the optical lattice potential in the same spatial dimension. $F = 0.5$, $V_3 = 1.0$, $g_1 = 1.5$ and $g_3 = 0.1g_1$

The V-K criterion of stability of the solution is $\frac{V_3 \sin\zeta\mathcal{L}}{g_3^2\zeta} - \frac{\mathcal{L}V_3}{g_3^2} > \frac{\mathcal{L}}{g_1}$. It is interesting to note that if $\zeta\mathcal{L} << 1$ then the solution will be stable if $\mathcal{L}/g_1 < 0$, or the two-body interaction requires to be attractive, which is opposite to the situation elaborated in the previous section.

From the study of the static solutions, it is evident that periodic density wave do exist, however to comment on the existence of supersolid phase it is necessary to study the dynamics of the solution and subsequent phase coherence. In the next section, we will investigate the analytical solution for a DCQNLSE loaded in a harmonic trap which is tightly confined in the transverse direction and the system is allowed to spread along the longitudinal axis. In the longitudinal direction, the system additionally experiences a BOL. We consider the dynamical solution to have both amplitude and phase. Through a systematic analysis we elaborate the behaviour of the phase and the amplitude.

4.2 Dynamic Solution

Next, we are interested to obtain an analytical solution derived from the time-dependent DCQNLSE (TDCQNLSE) and investigate on its temporal behaviour. We assume the TDCQNLSE with an additional harmonic confinement which is more amenable from the experimental point of view. Also it is worth noting that the use of harmonic trap along with other trapping potentials is a common practice to simulate realistic configurations of cold atoms experiments [76, 64]. The usual practice is to load the ultracold atomic system in a 3D harmonic trap and then carry out necessary modulation based on the experimental demand as in the case of supersolid observation [57]. In the experiment of supersolid the gas was first loaded in a cigar shaped trap which implies tight transverse confinement allowing the atoms to accommodate themselves only in the longitudinal direction ($\frac{1}{2}m\omega_{\perp}^2(y^2+z^2) >> \frac{1}{2}m\omega_0^2x^2$) [78, 79]. As mentioned earlier, typically $\omega_{\perp}/\omega_0 \sim 10$ allows us to achieve the cigar-shaped geometry. Here, we plan to explicate the analytical method to treat the TDCQNLSE in a cigar-shaped trap. We observe that the presence of harmonic trap in the system necessitates the presence of a chirped phase [80], which yields an efficient nonlinear compression at a desired parameter regime. In presence of a repulsive (regular) harmonic trap [80], the stripe phases lead to resonances. When the frequency of the chirped pulses is in resonance with the frequency of the harmonic trap, a significant increase in kinetic energy is observed, which gives rise to the nonlinear compression of the condensate [81].

4.2.1 Coherent Control

In our model, with reference to Eq.(2.6), we further assume that the longitudinal trap can breathe such that $K \equiv K(t)$ and the BOL is super imposed over the pulsating harmonic trap, $\frac{1}{2}K(t)x^2$, in the same spatial dimension. Additionally, we assume that the interaction strengths can be modulated temporarily such that the two body interaction is defined as $\mathcal{G}_1(t)$ and the beyond mean-field interaction can be defined as $\mathcal{G}_2(t)$. Hence, the TDC-

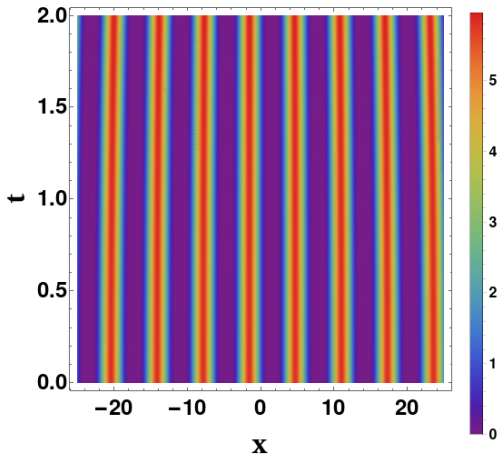

Figure 4.3: Time evolution of the stripe phase in presence of harmonic confinement of angular frequency, $K = 0.1$. The initial amplitude and position of the center of mass is assumed as 1 and 0.01 respectively. The potential depth is assumed to be $V_1 = 1$ and $\Lambda = 0.5$. We fix the two-body interaction strength as $g_1 = 1.5$ and the strength of the BMF contribution is $g_2 = 0.3g_1$. The parameter values are arbitrary in nature.

QNLSE can be described as:

$$i\frac{\partial\psi}{\partial t} - \mathcal{H}\psi = \mathcal{F}(x,t), \tag{4.10}$$

where, $\mathcal{H}(x,t) = -\frac{1}{2}\frac{\partial^2}{\partial x^2} + \frac{1}{2}K(t)x^2 + \mathcal{V}_{BOL}(x,t) + \mathcal{G}_1(t)|\psi|^2 + \mathcal{G}_2(t)|\psi|^3 - \nu(t)$. Here, $\nu(t)$ is the temporally modulated chemical potential. We assume an ansatz solution for Eq.(4.10) such that,

$$\psi(x,t) \;=\; \sqrt{\mathcal{M}(t)}\Phi[\xi(x,t)]e^{i[\varrho(x,t)+\Xi(x,t)]}, \tag{4.11}$$

$\varrho(x,t)$ describes the chirped phase and $\Xi(x,t)$ is the density dependent complex phase of the solution profile [28]. We assume that, the chirped phase has a quadratic form such that, $\varrho(x,t) = a(t) - \frac{1}{2}c(t)x^2$. The ansatz solution is described in the center of mass (COM) frame where we incorporate usual Galilean transformation such that $\xi(x,t) = \mathcal{M}(t)(x - l(t))$. Applying Eq.(4.11) in Eq.(4.10) and separating the real and imaginary

part of Eq.(4.10) result in two equations, commonly noted as, continuity (imaginary part) and pressure (real part) equation [82]. A set of consistency condition emerges from the above mentioned equations such that,

$$\frac{d\mathcal{M}}{dt} = \mathcal{M}c;\ cl + \frac{dl}{dt} = \Lambda\mathcal{M};\ \mathcal{G}_1(t) = \mathcal{M}g_1;\ \mathcal{G}_2(t) = \sqrt{\mathcal{M}}g_2;$$
$$\mathcal{F} = \mathcal{M}^{5/2}F\sin\xi(x,t);\ \mathcal{V}_{BOL}(x,t) = \mathcal{M}^2V(\xi(x,t));\ \nu(t) = \mathcal{M}^2\mu \quad (4.12)$$

Here, Λ plays a role equivalent to velocity. The presence of the trap necessitates chirping of the phase [82], which enforces another velocity component. In the absence of the trap, it is appropriate to consider $c(t) = 0$ then we can easily derive that $l(t) = \Lambda t$ [82]. The equation of motion of the COM can also be noted as

$$\frac{d^2l(t)}{dt^2} + Kl(t) = 0. \quad (4.13)$$

This implies that the oscillation frequency of the COM is same as the trap. Thus for a regular harmonic oscillator trap with constant K we obtain $l(t) = l_0\sin\sqrt{K}t$. Here, l_0 describes the position of the COM. If K is a periodic function of t, then the COM follows Mathieu function solution [83].

It is possible to determine $c(t)$ from a Riccati type equation [28] such that $\frac{dc}{dt} - c^2 = K$ which can be mapped to Schrödinger equation, through a transformation $c(t) = -\frac{d\ln b(t)}{dt}$. Additionally, it can be shown that $a(t) = \lambda\int_0^t \mathcal{M}^2dt'$, where λ is an arbitrary constant.

The equation of continuity leads to the following phase relation,

$$\frac{d\Xi}{d\xi} = \Lambda - \frac{2C_0}{\Phi^2}. \quad (4.14)$$

To avoid the amplitude dependence on the phase [82], we consider the integration constant $C_0 = 0$. Hence, we can rewrite the amplitude equation such that,

$$-\frac{\lambda}{2}\Phi + \Lambda\Phi\Xi_\xi + F\sin\xi = -\frac{1}{2}\left(\Phi_{\xi\xi} - \Xi_\xi^2\Phi\right) + V(\xi)\Phi + g_1|\Phi|^2\Phi + g_2|\Phi|^3\Phi - \mu\Phi. \quad (4.15)$$

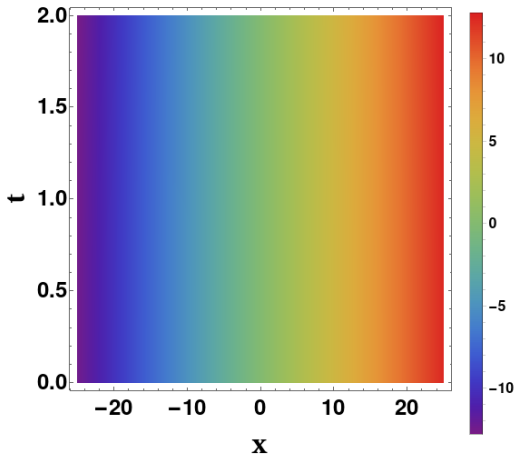

Figure 4.4: The figure depicts the spatio-temporal variation of the phase. The parameter values used for this plot is same as Fig. 4.3 and they are arbitrary in nature.

This implies,

$$-\frac{1}{2}\Phi_{\xi\xi} + V(\xi)\Phi + g_1|\Phi|^2\Phi + g_2|\Phi|^3\Phi - \tilde{\mu}\Phi = F\sin\xi \tag{4.16}$$

Here, $V(\xi) = V_2\sin\xi - V_1\sin^3\xi$ and $\tilde{\mu} = \left(\mu + \frac{\Lambda}{2} - \frac{\lambda}{2}\right)$. It must be noted here that Eq.(4.16) and Eq.(4.2) are of the same structure. Thus an ansatz solution of the form $\Phi(\xi) = A + B\sin\xi$ will yield same result as before. This is a very important aspect of our scheme, which allows the dynamical equation to cast itself in the same form like the static equation. Hence, it is obvious to conclude that the solutions of time-dependent DQC-QNLSE and DQCNLSE will have same solution as their static counterpart only differing in the frame of reference of the solutions.

Let us consider the simplest possible situation, where the trap frequency is not pulsating i.e., $K(t) \equiv K$. This leads to a trivial solution of the Riccati equation such that $c(t) = \sqrt{K}\tan\sqrt{K}t$. Subsequently, one can derive $\mathcal{M}(t) = \mathcal{M}_0\sec\sqrt{K}t$. Here $\mathcal{M}_0$ the amplitude of the COM of the system at $t = 0$.

The actual solution inside the trap leads to the striped phase as depicted in Fig. 4.3. The corresponding phase can be derived using Eq.(4.14) and it has been depicted in Fig 4.4.

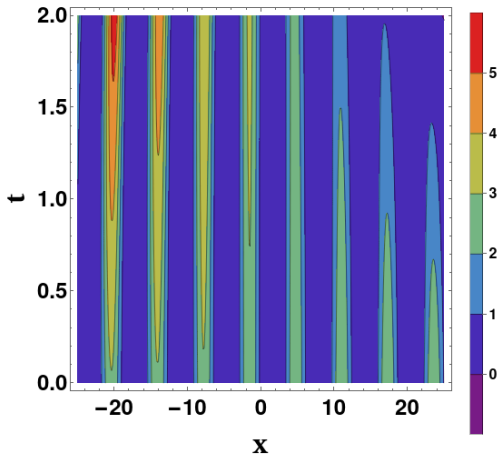

Figure 4.5: The spatio-temporal variation of super current is depicted here. The appearance of supercurrent coincides with the stripes. In the figure the longitudinal trap frequency $K = 0.1$, the lattice depth is considered as $V_1 = 1$. The amplitude and position of the COM at $t = 0$ is assumed as 1 and 0.01 respectively. The MF and BMF interaction strengths are noted as $g_1 = 1.5$, $g_2 = 0.3g_1$. The parameter values are chosen arbitrarily.

The moderate spatio-temporal phase variation in the figure points to the phase coherence. The figure clearly suggests that the temporal coherence is retained whereas marginal fluctuations in the spatial coherence. Thus, the existence density wave illustrated via striped phase and possible phase coherence can be attributed to the emergence of supersolidity. Hence, our formalism provides an alternative route to achieve the supersolid phase without using the dipolar BEC, rather applying a calibrated external driving force.

4.2.2 Superfluid Current and Density

It is now quite instructive to calculate the supercurrent as $\mathcal{J}(\xi) = \mathcal{M}(t)^2\Phi(\xi)^2\,[-c(t)x + \Lambda]$. The calculation of supercurrent plays pivotal role in understanding the dynamical superfluid insulator transition (DSIT). It must be noted here that, DSIT has a classical nature driven by modulational instability and is quite different from the fluctuation-driven quantum phase transition [84, 85, 86]. The behaviour of the supercurrent is shown in Fig 4.5. We observe that the DSIT occurs in this system also similar to Ref.[86], where the atoms transit from the superfluid phase to an insulating phase, with periodicity analogous to the stripes de-

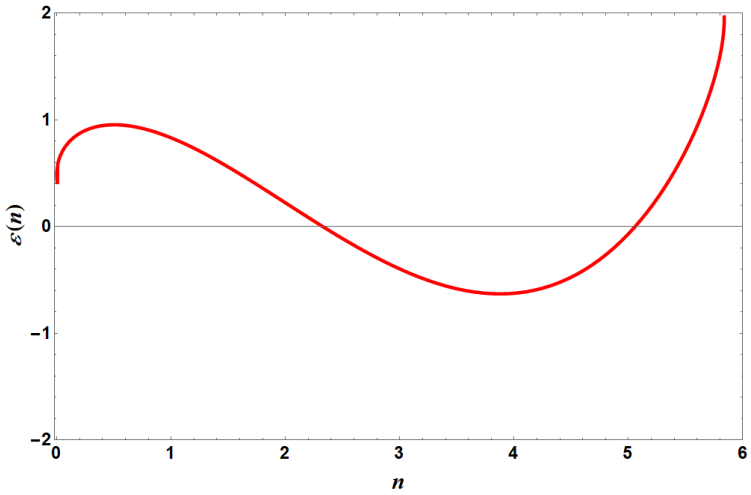

Figure 4.6: The figure describes variation of energy functional as a function of density. The figure is prepared at $t = 0$ and we have used $\mathcal{M}_0 = 1$, $l_0 = 0.01$, $K = 0.1$, $\Lambda = 0.5$, $V_1 = 1$, $g_1 = 1.5$ and $g_2 = 0.3g_1$. The values are chosen arbitrarily however they are consistent with the values used to prepare the earlier plots.

scribed in Fig 4.3. The insulating phase wavefunction corresponding to $\mathcal{J}(\xi) = 0$ can be noted as $\Phi_I(\xi) = \frac{g_1}{3g_2} \sin \xi$.

Off late it has been shown that quantum stabilization results in the formation of quantum droplets [55] and it is possible to form regular arrays of droplets in presence of a trap. However, due to lack of phase coherence they can not be immediately classified as supersolid [55]. Nevertheless, the close association of droplet to supersolid is an undeniable fact. In this work we have presented analytical scheme to derive stripe phase solution and explicated their phase coherence. Yet we have not investigated the situation from the prospect of self-bound droplets which additionally show phase coherence. To study the droplet bound state, it is required to calculate the energy functional. The energy functional of the condensate can be expressed as [87]:

$$\varepsilon(n) = \frac{1}{2}\left|\frac{d\psi}{dx}\right|^2 + \left(\frac{1}{2}Kx^2 + \mathcal{V}_{BOL} - \nu(t)\right) n + \frac{1}{2}\mathcal{G}_1 n^2 + \frac{2}{5}\mathcal{G}_2 n^{5/2}, \tag{4.17}$$

where $n = |\psi|^2$. The terms on the right-hand side, corresponds to the kinetic energy, the potential energy due to both harmonic and OL confinement, chemical potential and interaction potentials are noted. The interaction potentials include usual MF contribution as well as the BMF contribution. Fig. 4.6 described the variation of energy functional with density at $t = 0$. Contrary to the usual energy functional diagram of droplets, we observe that the energy is nonzero at very low density. However, a gradual drop in energy is observed with increase in density. The trajectory clearly suggests the existence of two critical densities (cd) of n_{cd_1} and n_{cd_2} such that $n_{cd_1} < n_{cd_2}$. According to the figure, the energy becomes negative beyond $n_{cd_1} \sim 2.34$ thereby suggesting formation of self-bound droplets. Further increase in density leads to the equilibrium point where the quantum pressure is zero. This density can be noted as $n_{eq} \sim 3.88$ and the energy is lowest at this point. Thereafter the energy starts to grow with increase in density and it becomes positive after $n_{cd_2} \sim 5.06$ indicating that the scope of bound droplets formation is exhausted beyond this point. Here, one must corroborate with the density favourable for bound state formation with the density described in Fig 4.3. In Fig 4.3 we can note that the stripe density varies is varying between ~ 2 to ~ 5.5 which also quite close to the stripe density range ($n_{cd_1} \leq n \leq n_{cd_2}$) where the energy functional is negative as described in Fig 4.6.

Now, integrating the energy functional along with the driving force, as noted in Eq.(4.18), over one period of the lattice potential [88], we obtain the total energy of the system,

$$E(t) = \int (\varepsilon(n) - \mathcal{F})\, dx. \tag{4.18}$$

The expression for the energy is vast and unwieldy to mention, but we can obtain the energy spectrum as described in Fig. 4.7. It shows rapid nonlinear resonant increase in energy of the condensate trapped in a harmonic and BOL potential. Rapid nonlinear compression can be seen at certain values of the time variable [48], imitating the occurrence of resonances in this system. These nonlinear resonances occur periodically at the point of nonlinear compression [48] of BEC, where the density takes its maximum value. The contribution of the quadratic chirped phase to the kinetic energy is solely responsible for this phenomenon

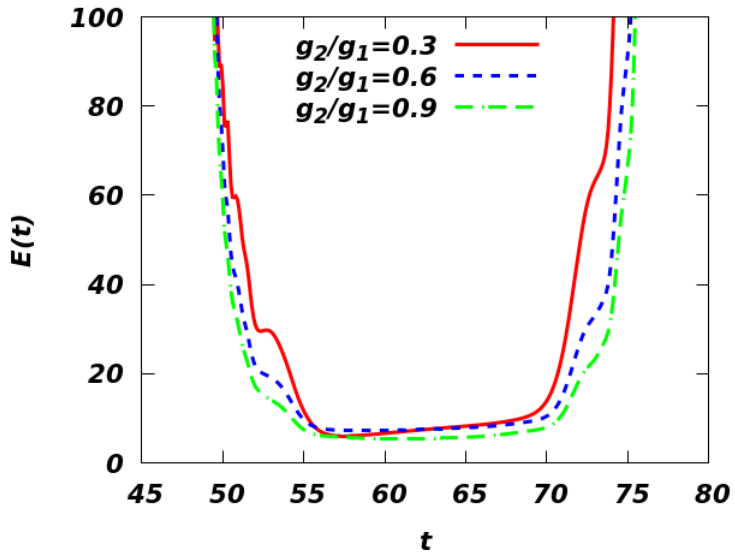

Figure 4.7: The energy spectrum is shown when both harmonic confinement and the BOL is active for different interaction strengths. There is no significant variation due to change in interaction. The parameter values remain same as previous such that $\mathcal{M}_0 = 1, l_0 = 0.01$, $K = 0.1, \Lambda = 0.5, V_1 = 1$.

[48, 81]. In other words, the resonances occur when the driving frequency of the potential and external force matches with the natural frequency of the system. The resonant behaviour remains same for different interaction ratio between g_1 and g_2. This is akin to the observed resonant behaviour in an OL [89].

4.3 Concluding Remarks

In this chapter, we have studied DCQNLSE and evaluated its periodic solution which is analytical in nature. The application of this type of system is a Q1D BEC where competition between MF and BMF interaction allows formation of droplets. We then extend our analysis to DQCNLSE to capture the dimensional crossover and effect of BMF interaction. However, in DQCNLSE we observe the wave function itself is different. Thus, break down the possibility of any analytical continuation from Q1D to 1D regime. We checked the stability of obtained solutions via VK criterion and noted that the solution remains stable if

the two-body MF interaction is repulsive.

Later we explicate the dynamics of DCQNLSE in presence of a harmonic as well as BOL potential. The emergence of stripes becomes quite evident, and we study the phase coherence as well. The corresponding energy calculation indicates the existence of critical bound of densities which appears to be favourable for bound state formation. These critical densities are very similar to the stripe densities.

Chapter 5

Droplet Solution In Homogeneous System

Here, we plan to analytically analyze the two component BEC in Q1D system as described in Fig. 2.1. At this juncture, it is worth mentioning that a numerical investigation of quantum liquid in for dipolar BEC in Q1D geometry has very recently been reported [61]. Our focus also gels well with the current interests on droplets at lower dimension which includes, a comprehensive analysis on the role of LHY term in suppressing the collapse in quasi two- dimensional system [90]. Of late, a possible connection has also been drawn between the droplets and modulational instability in 1D [91].

Our primary goal is to find out an analytical solution for Q1D CQNLSE in homogeneous case. The next objective is to explore the droplet state. Here we note that, in chap. 3, we have proposed cnoidal solutions of a generic CQNLSE [34]. There, we have used a cnoidal potential to stabilize the analytical solutions.

In this chapter, we specifically focus on (i) obtaining an analytical solution of Q1D CQNLSE in homogeneous environment; (ii) validation of the analytical solution through numerical calculation via split-step Crank-Nicolson (CN) method; (iii) investigation of the stability for the obtained solutions via VK criterion [47]; (iv) linear stability analysis which includes investigation of modulational instability [92]; (v) examination of the droplet region using the analytical solution where we calculate the equilibrium density and critical density of the liquid-like state. The equilibrium density is noted as the transition point between bright soliton-like state to stable liquid like state. The critical density, beyond which the

droplets disappear, is calculated and corroborated with the theory. We also demonstrate the existence of a density plateau for higher number of particles signifying the creation of quantum liquid.

Here, by stating a Q1D system, we assume that $\sqrt{na^3} < 1$ however $\frac{1}{|\sqrt{n_{1D}a_{1D}}|} > 1$ [71]. Nevertheless, our objective is to remain more towards the right side of the dimensional crossover where as a strict 1D system is more towards the left of the crossover where $\frac{1}{|\sqrt{n_{1D}a_{1D}}|} < 1$ as suggested in Ref. [71]. As mentioned earlier, mathematically a Q1D system leads to a CQNLSE where as a 1D system can be described by a QCNLSE [38].

5.1 Solutions

In this section, our main focus is to explicate the interplay between EMF and BMF interactions hence we exclude the effect of harmonic confinement and the system can become quasi-homogeneous. Experimentally the system can be reduced to a quasi-homogeneous setup by considering transverse confinement is much stronger compared to the longitudinal confinement ($\omega_0 << \omega_\perp$) resulting $K \to 0$. The next objective is to obtain analytical solution for Eq.(2.6) assuming $K = 0$.

In this section, we elaborate on the mathematical scheme to derive the analytical solution for Q1D CQNLSE and analyze the stability of the obtained solutions. To start with, we write the wave function such a way that, $\psi(x,t) = \rho(x,t)\exp\left[i\left(\chi(x,t) + \mu_0 t\right)\right]$ where $\rho(x,t)$ leads to the amplitude contribution and $\chi(x,t)$ is the non-trivial phase, μ_0 being the chemical potential. Applying this ansatz in Eq.(2.6) we yield two equations, namely imaginary and real equation respectively such that,

$$\rho_t = -\chi_x\rho_x - \frac{1}{2}\chi_{xx}\rho \tag{5.1}$$

$$-\chi_t\rho = -\frac{1}{2}\left(\rho_{xx} - \chi_x^2\rho\right) + \mathcal{G}_1\rho^3 + \mathcal{G}_1\rho^4 + \mu_0\rho. \tag{5.2}$$

Eq.(5.1) leads to the continuity equation and if we transform the equation in COM frame,

i.e., $\zeta = x - ut$, then we obtain,

$$\chi_\zeta = u + \frac{C_0}{\rho^2}. \tag{5.3}$$

Here, u defines the velocity of the wave and C_0 is the integration constant. Eq.(5.2) in the comoving frame can be rewritten as,

$$\chi_\zeta u\rho = -\frac{1}{2}\left(\rho_{\zeta\zeta} - \chi_\zeta^2\rho\right) + \mathcal{G}_1\rho^3 + \mathcal{G}_2\rho^4 + \mu_0\rho. \tag{5.4}$$

Applying Eq.(5.3) in Eq.(5.4) we obtain,

$$\begin{aligned} \rho_{\zeta\zeta} + (u^2 - 2\mu_0)\rho - 2\mathcal{G}_1\rho^3 - 2\mathcal{G}_2\rho^4 &= 0 \\ \text{or, } \frac{d^2\rho}{d\zeta^2} + \left(g\rho^2 - g'\rho^3 + 2\Upsilon\right)\rho &= 0. \end{aligned} \tag{5.5}$$

To derive Eq.(5.5) it is important to consider that the phase and amplitude are uncorrelated which allows us to set $C_0 = 0$ [82]. We also note that $\Upsilon = u^2/2 - \mu_0$. Further, we assume $g = -2\mathcal{G}_1$ and $g' = 2\mathcal{G}_2$ implying a two-body EMF interaction is attractive and LHY contribution is repulsive. The minimum criterion for droplet formation is that these two interactions must be competing. Otherwise, we will not be able to see any qualitative change in the behavior of the system.

We consider an ansatz solution such that,

$$\rho(\zeta) = \frac{A}{1 + \sqrt{1 - A}\cosh(\sqrt{\xi}\zeta)}, \tag{5.6}$$

where $\sqrt{\xi}$ is the inverse of coherence length. Applying the ansatz in Eq.(5.5) we obtain a set of condition for which Eq.(5.6) is a solution of Eq.(5.5). The constrained conditions

read,

$$\begin{aligned} A &= \frac{-\xi \pm \sqrt{-6\Upsilon g + 3g\xi + \xi^2}}{g}, \\ \xi &= 6\Upsilon + g, \\ \Upsilon &= \frac{g' - g}{2}, \\ |g| &= 2g', \text{ or } |g| = 3g'. \end{aligned} \tag{5.7}$$

The last equation in Eq.(5.7) implies that it is possible to obtain an analytical solution if and only if the BMF interaction is half or one third (i.e. $g' = |g|/2$ or $|g|/3$) of the EMF interaction and repulsive in nature. Hence, we can write the solutions as,

$$\rho(\zeta) = \frac{12\mu_g}{1 + \sqrt{1 - 12\mu_g}\cosh\left(\sqrt{\frac{g}{2}}\zeta\right)} \text{ for } |g| = 2g' \tag{5.8}$$

$$= \frac{1 + 12\mu_g}{1 + \sqrt{12\mu_g}\cosh\left(\sqrt{g}\zeta\right)} \text{ for } |g| = 3g'. \tag{5.9}$$

Here, $\mu_g = \mu_0/g$. Using the constrained conditions, we can also evaluate ξ which is actually related to the two-body interaction via $\xi = -|g|/2$ or $-|g|$. This implies that the localized structures can only sustain if and only if $g < 0$ or the EMF interaction is attractive. We must note here that for real solution, $\mu_g > 0$, $\mu_0 < 0$ and correspondingly $\Upsilon > 0$. In the subsequent discussions we will use $|g| = 1$ for uniformity. The effect of variation of $|g|$ is discussed in detail in chap. 6.

Here, our major objective is to understand the interplay between EMF and BMF interaction for the formation of droplets and the role of chemical potential. Hence, we define the relationship between normalization N and chemical potential μ_0 as,

$$N = \begin{cases} \sqrt{\frac{2}{g}}\left[\sqrt{\mu_I}\ln\left[\frac{2\sqrt{\mu_I}}{\sqrt{\mu_I}-1} - 1\right] - 2\mu_I\right] \\ \frac{(1+\mu_I)^2}{\sqrt{g}(1-\mu_I)}\left[\ln\left[1 - \frac{2}{\mu_I}\left(\sqrt{1-\mu_I}+1\right)\right] - 2\right] \end{cases} \tag{5.10}$$

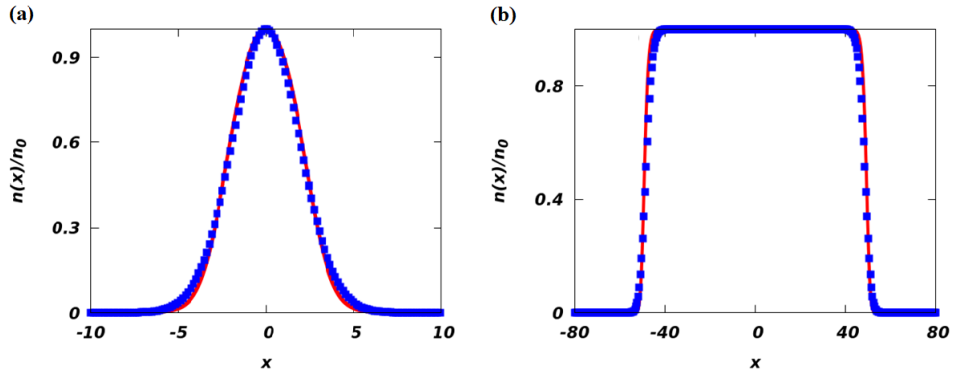

Figure 5.1: The figures described the comparison between the obtained analytical solution using Eq.(5.9) and numerical solution of Eq.(2.6). The solid red line described the analytical result and the blue squares represents numerically obtained solution. (a) depicts the low particle number solitonic regime (figure created for $N = 4$) and (b) described high particle number ($N = 100$) droplet regime. The density is normalized by n_0 where n_0 is $n(x)|_{x=0}$.

Here, the first equation derived from Eq.(5.8) (assuming $\mu_I < 1$). Likewise, N is again calculated from Eq.(5.9) and noted in the second equation. We also recall that $\mu_g = \mu_0/g$ and for the convenience of calculation we have denoted, $12\mu_g = \mu_I$. N can also be noted as the number of particles associated with the formation of localized wave.

5.2 Numerical Analysis

Now, we corroborate our analytical result with numerical simulation. For this purpose, split-step CN method with imaginary time propagation is quite useful. It is well accepted that, for stationary ground states, imaginary-time propagation method is very accurate and convergence is quite fast. This method also happens to be very robust. Hence, we employ the CN algorithm following Ref.[93] for our model. In Fig. 5.1, we compare the analytical and numerical result where the solid red line is our analytical solution from Eq.(5.9) and the blue solid squares are the numerically obtained solution of Eq.(2.6). Fig. 5.1(a) and (b) corresponds to bright soliton like state ($N = 4$) and liquid like state ($N = 100$) respectively.

Since, our analytical solution is constrained through a relationship between MF and

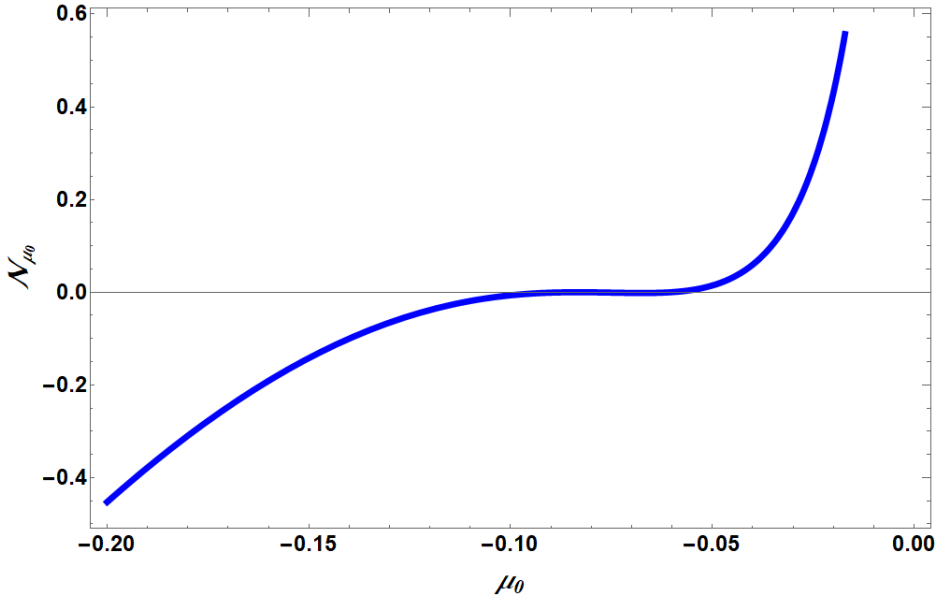

Figure 5.2: The stability criterion is inspected for the solution described in Eq.(5.9) which depicts a zero crossing at $\mu_0 = -0.06$ for $|g| = 1$.

BMF interaction strength ($|g| = 2g'$ and $3g'$) thus we can use our numerical result for variety of interaction parameters to study BMF phenomena more closely. We did check our numerical solution for $\kappa = g'/|g| = 0.1, 0.5$ and 0.8 starting with a seed solution such as, sech(x). The results are in accordance with our understanding of the role played by BMF interaction such as progressive flattening of density with increasing BMF interaction strength.

5.3 Stability Analysis

Before proceeding to any discussion related to droplet formation, it is important that we evaluate the stability of the obtained solutions. For this purpose, we intend to employ the well-known VK criterion [47].

In order to obtain the stability criterion of the given solutions, we calculate $\mathcal{N}_{\mu_0}$ from Eq.(5.8) as well as Eq.(5.9) as $\mathcal{N}_{\mu_0} = \frac{\partial N}{\partial \mu_0}$. A primary inspection leads to the conclusion that the first case or Eq.(5.8) does not lead to any stable solution. However, it's possible to

obtain a region where $\mathcal{N}_{\mu_0}$ is positive thereby suggesting a stable solution regime from the second solution or Eq.(5.9). The behavior of $\mathcal{N}_{\mu_0}$ is noted in Fig. 5.2. We find the threshold value at -0.06 after which $\mathcal{N}_{\mu_0} > 0$. However, $\mathcal{N}_{\mu_0}$ diverges as $\mu_0 \to 0$. We are unable to find any region of stability for positive μ_0.

Next, we perform the linear stability analysis of the second solution. In realm of linear stability analysis our first objective is to calculate the modulational instability (MI) where the applied perturbation is considered as plane waves. It must be noted that MI plays a crucial role in nonlinear systems and quite recently through a remarkable experiment it was shown that soliton trains were created by the MI [94]. Only a few months back, the role of MI has been discussed in the context of droplet formation in a purely 1D system [91]. A systematic analysis of MI can reveal the region of instabilities in the parameter space.

Here, we apply a small perturbation to the stationary solution such that, $\psi(x,t) = \psi_0(x) + \delta\psi(x,t)$ provided, $\delta\psi << 1$. Now, substituting the solution in Eq.(2.6) (with $K = 0$) and linearizing it, one obtains the eigenvalue equation in terms of the perturbation $\delta\psi$,

$$i\frac{\partial\delta\psi}{\partial t} = -\frac{1}{2}\frac{\partial^2\delta\psi}{\partial x^2} + g(2n\delta\psi + n\delta\psi^*) + g'(3n^{3/2}\delta\psi + n^{3/2}\delta\psi^*). \tag{5.11}$$

Eq.(5.11) is commonly known as Bogoliubov-de Gennes (BdG) equation [95], where $n = |\psi_0|^2$. A further decomposition of $\delta\psi$ in real and imaginary part leads to,

$$\begin{aligned} &\begin{pmatrix} -\frac{1}{2}\partial_{xx} + Q_1(g,g',n) & 0 \\ 0 & -\frac{1}{2}\partial_{xx} + Q_2(g,g',n) \end{pmatrix} \begin{pmatrix} \delta\psi_R \\ \delta\psi_I \end{pmatrix} \\ = &\begin{pmatrix} 0 & 1 \\ -1 & 0 \end{pmatrix} \partial_t \begin{pmatrix} \delta\psi_R \\ \delta\psi_I \end{pmatrix}. \end{aligned} \tag{5.12}$$

Here, $Q_1(g,g',\psi_0) = gn + 2g'n^{3/2}$ and $Q_2(g,g',\psi_0) = 3gn + 4g'n^{3/2}$. Assuming, $\delta\psi =$

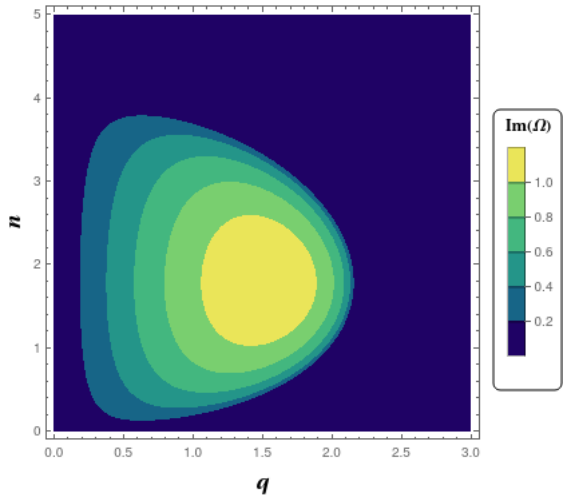

Figure 5.3: Im(Ω) or MI gain is plotted as a function of density and wavenumber using Eq.(5.14).

$\begin{pmatrix} \delta\psi_R \\ \delta\psi_I \end{pmatrix} = e^{i(qx-\Omega t)}$, one can yield the perturbation eigenmodes where q denotes the wavenumber and Ω stands for frequency. The resulting dispersion relation can be noted as $\Omega^2 = (\frac{q^2}{2} + 3gn + 4g'n^{3/2})(\frac{q^2}{2} + gn + 2g'n^{3/2})$ which boils down to

$$\Omega^2 = \frac{q^4}{4} + q^2(2gn + 3g'n^{3/2}), \tag{5.13}$$

by taking into account only the q dependent terms in the dispersion relation. Further, inserting the existing relationship between g and g' the dispersion relation described in Eq.(5.13) can further be simplified as,

$$\Omega^2 = \frac{q^4}{4} + q^2|g|n(2 - \sqrt{n}). \tag{5.14}$$

It is evident from Eq.(5.14) that the dispersion is dependent on the sign of the right hand side expression. If positive, then Ω will be real, corresponding to mere oscillations around the unperturbed solution, however if negative, the frequency will become imaginary, corresponding to exponential growth and thus instability. Therefore, instability will occur

when $\frac{q^4}{4} + q^2|g|n(2-\sqrt{n}) < 0$. Hence, if we denote $\Gamma = \text{Im}(\Omega)$ as MI gain then in the stable region $\Gamma = 0$ where as in the unstable region $\Gamma \neq 0$. Fig.5.3 draws the contours for $\Gamma \neq 0$ as a function of wavenumber and density. This reveals that at low density region till $n \sim 4$ system experiences instability. From Eq.(5.14), one can also conclude that the system is unstable for $q^2 < 4|g|n(2-\sqrt{n})$.

5.4 Quantum Droplet

The signature of droplet formation can be obtained from the spatial profile of the obtained solution which we provide in Fig. 5.4. The figure depicts the characteristic static density profile of Eq.(5.9). However, the chemical potential μ_0 is obtained by numerically solving the second equation of Eq.(5.10) for different norm (N) at a fixed EMF ($|g| = 1$). We observe a non-uniform shape for small N where kinetic energy actually relevant for determining the shape as quantum pressure dominates over the potential energy. The situation is analogous to usual single component bright soliton solution with cubic nonlinearity. However, as we increase N we start observing a flattening of the top or accumulation of uniform density. This signature is observed for $N \geq 10$ and it reminds of a classical liquid where density starts becoming spatially uniform with progressive accumulation of droplets. In the figure we have normalized all the profiles by peak density ($n_0 = n(x=0) = \left|\frac{1+12\mu_g}{1+\sqrt{12\mu_g}}\right|^2$), which also happens to be the bulk value. It is evident from the figure that for higher N the density plateau approaches the constant bulk value of n_0.

It must be noted here that similar observation of density plateau is already reported in Ref.[63]. However, the density plateau was noted for 1D system which implies the governing equation was a quadratic-cubic NLSE or QCNLSE, whereas in this investigation we have concentrated on a Q1D system resulting a dynamical equation governed by cubic-quartic nonlinearities which we name CQNLSE. Another important differentiator is the nature of the nonlinearities. In the mentioned reference the quadratic and cubic nonlinearities are attractive and repulsive, respectively. In comparison, we obtain our solution for attractive cubic and repulsive quartic nonlinearity. It must be noted that the interaction

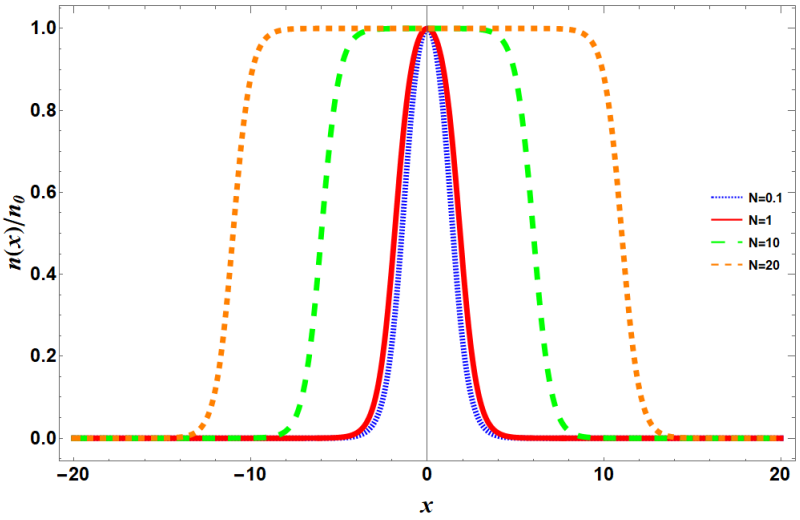

Figure 5.4: The stationary density profile ($n(x) = |\rho(x)|^2$) corresponding to Eq.(5.9) is depicted here. The blue dotted line, red solid line, green large dashed and orange short dashed lines correspond to $N = 0.1, 1, 10, 20$ respectively. The density is normalized by n_0 where n_0 is $n(x)|_{x=0}$.

strength of similar nature was involved in the experimental observation of quantum liquid in binary condensate [5].

As noted above, the potential energy plays the dominating role over the kinetic energy when the droplets start to accumulate and create a puddle. Thus, we concentrate on the effective potential energy which can be defined as, $\mathcal{E}_I = 1/2gn^2 + 2/5g'n^{5/2}$. The first term is derived from the EMF interaction and the second term is BMF contribution. If both the interactions have the same sign, no qualitative change in behavior occurs. However, the system can exhibit novel behavior if the interactions are competing as discussed in this work. When the EMF interaction is low then BMF corrections are not necessarily negligible. Now at low density the quantum depletion remains negligible, so the approximation upto LHY-level remains valid. Since in our case $g < 0$ but $g' > 0$, thus $\mathcal{E}_I = -1/2gn^2 + 2/5g'n^{5/2}$ describes the actual effective potential. The situation is mimicked in Fig. 5.5 where the green dashed-dotted line described the attractive EMF interaction and red dashed line depicts the repulsive BMF interaction. The resultant interaction is represented by a yellow short dashed line which is initially negative at low density but slowly grows and becomes

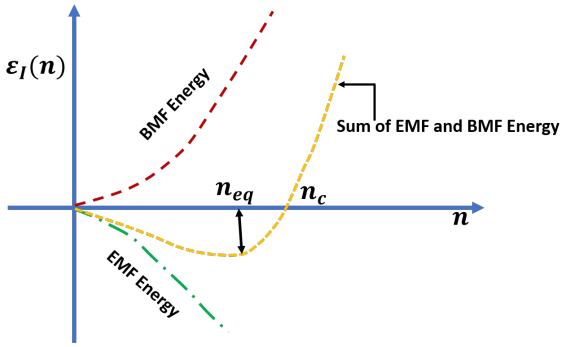

Figure 5.5: The attractive (EMF) and repulsive (BMF) interactions are depicted schematically. This creates an effective non-monotonic interaction. The density corresponding to the base of the effective interaction curve describes the equilibrium density (n_{eq}) and the nonzero density at which effective interaction becomes zero is defined as critical density (n_c).

positive at relatively higher density. The level crossing point is defined as the critical density (n_c) after which the droplets are expected to collapse. This point can be evaluated by inserting $\mathcal{E}_I = 0$ and it turns out, $n_c = \frac{25}{16}\frac{g^2}{g'^2} = 14.06$ (since, $g' = |g|/3$) which matches exactly with Fig. 5.6.

The minimum of the interaction resultant signifies the equilibrium density (n_{eq}). At this point the pressure is zero which implies $\mathcal{P} = \mathcal{E}_I - n\frac{d\mathcal{E}_I}{dn} = 0$, resulting $n_{eq} = \frac{25}{36}\frac{g^2}{g'^2} = 6.25$. However, in Fig. 5.6 the minimum is at about 8.94. As the equilibrium density signifies the point from where the solitons start combining together to form the droplet as BMF effect takes over the EMF effect therefore to understand this anomaly is important. Hence, we analyze the chemical potential. The critical chemical potential (μ_{g_c}) and equilibrium chemical potential ($\mu_{g_{eq}}$) can be expressed from effective potential energy as, $\frac{25}{64\kappa^2} = 3.51$ and $-\frac{25}{216\kappa^2} = -1.04$ respectively. Using n_c value from Fig. 5.6 if we recalculate μ_{g_c} as $\mu_{g_c} = -n_c + \kappa n_c^{3/2}$, we obtain a good agreement. The equilibrium chemical potential or $\mu_{g_{eq}}$ from Fig. 5.6 turns out as -0.02. Solving Eq.(5.10) numerically, we also observed that when N is relatively large $\mu_g \to 0^-$ resulting the emergence of flat plateau as shown in Fig. 5.4. Hence, the equilibrium density obtained from Fig. 5.6 corroborates well with the numerical result yet the departure from the theoretical value can be attributed to the

constrain condition which defines existence of exact solution only for $|g|/g' = 3$.

Nevertheless, it is well accepted that the signature of plateau is one of the important evidence of formation of the liquid-like state [3]. Hence, it is now possible to conclude that the droplet formation starts from the equilibrium point of density where the negative energy supports the bound state formation and further accumulation of particle happens as we increase the density till the point of n_c. The left-hand side of n_{eq}, i.e., $n < n_{eq}$, describes the bright soliton-like localized states as described in Fig. 5.4. Albeit, the system will collapse for $\mu_g = -1.5$ as solving $\mu_g = -n + \kappa n^{3/2}$ for density leads to the condition of $\mu_g = -\frac{1}{6\kappa^2}$ when the density collapses. One must also note here that the solution is stable in the vicinity of the liquid-like state as stability criterion leads to $-0.06 \leq \mu_0 \leq 0.0$ for unit $|g|$.

Since $\mathcal{E}_I$ has explicit dependence on density and the interaction strength, therefore a variation of μ_g does not make any significant change in $\mathcal{E}_I$ as shown in Fig. 5.6. Another noteworthy point in our calculation is that, though the liquid formation starts from negative chemical potential however, the chemical potential corresponding to critical density is positive. This is a notable departure from the existing understanding of quantum droplets, however, from a stability point of view, the solution is not stable for positive chemical potential.

5.5 Concluding Remarks

A close inspection of the second solutions allows us to comment on the self-bound droplets as well as liquid like state. The static profile of the droplets reveals a density plateau for a higher particle number. We further analyze the effective potential energy and realize that the equilibrium chemical potential corroborates well with the numerically obtained chemical potential for flat spatial density. Moreover, the analytical solution is stable in the region where the droplets form. We also see that the critical density obtained via effective potential energy and from the analytical solution do match exactly.

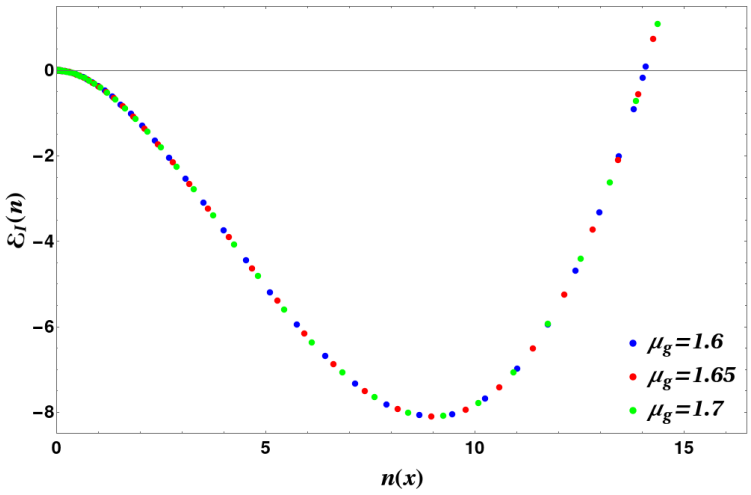

Figure 5.6: Interplay of EMF and BMF energy resulting in droplet formation in low density using Eq.(5.9). Here, the EMF energy is attractive and the LHY contribution is repulsive. Also, we can note that the critical density is unaffected by the different μ_g values.

Chapter 6

Droplet to Soliton Transition In Inhomogeneous System

In the previous chapter, we have proposed an exact analytical solution for the droplet-like state in a Q1D quasi-homogeneous cigar shaped BEC where we have assumed the longitudinal confinement is sufficiently weak so that it can be neglected [60]. We have also commented on the soliton to droplet transition. However, from an experimental perspective, it is more prudent to consider the cigar shaped harmonic confinement in Q1D as depicted in Fig. 2.1. Tuning the confinement potential should yield additional features that may be worth exploring [96]. So, we start with an expectation of finding some novel consequences by tuning the trapping potential. Our systematic analysis reveals that, the trap frequency indeed plays a significant role in understanding the droplet-soliton transition.

At this juncture, we also recall a numerical investigation of quantum liquids for the dipolar BEC in Q1D geometry [61]. Apart from that, we have also seen considerable interest in analysing the origin of the droplets in lower dimensions [90, 97]. A contemporary study also notes possible connection between the droplets and modulational instability in 1D system [91].

In this chapter, we look into the role played by the trap potential in droplet formation and possible transition from a droplet to a solitonic state via tuning the confinement potential. We report a droplet to a soliton crossover by tuning the external confinement potential

in a dilute BEC by solving numerically the inhomogeneous CQNLSE. The testimony of such a crossover is presented via studying the fractional density of the condensate which smoothly migrates from being a flat-head curve at weak confinement to a bright soliton at strong confinement. Such a transition occurs across a region of the potential whose strength varies over an order of magnitude and thus should be fit to be termed as a crossover. We supplement our studies via exploring the size of the bound pairs and the ramifications of the particle density therein. Eventually, all of these aid us in arriving at a phase diagram in a space defined by the trap strength and the particle number that shows the formation of two phases consisting of droplets and solitons, along with a regime of coexistence of these two.

To explicate the role of K in dropleton-soliton transition, we solve Eq.(2.6) numerically for different values of K. The numerical scheme involved a split-step CN method with imaginary time propagation [93]. In Sec. 6.1, first the effect of the longitudinal trapping potential for constant number of particles at different values of the BMF interaction strength is investigated. Later we extend our analysis toward the role of particle number and draw phase diagram. This allows us to comment on the nature of droplet to soliton transition.

We have already tested our numerical scheme, by comparing with the analytical result as depicted in Figs. 5.1 using Eq.(5.9) for $K = 0$. The computation appears in consonance with the analytical result and thus the scenario encourages us to proceed towards our actual objective of solving Eq.(2.6) with $K \neq 0$.

6.1 Droplet to Soliton Transition

We employ the imaginary time propagation method over small time steps (5×10^{-6}) for total 20000 steps and solve the inhomogeneous CQNLSE for several trap frequencies and different BMF interaction strengths. We introduce the interaction strength in terms of $\tau = \mathcal{G}_2/|\mathcal{G}_1|$ and we perform numerical calculations for three arbitrary values of τ, such that $\tau = 0.1, 0.5$, and 0.9. Here, it must be noted that in Ref.[60], the analytical solution was obtained for $\tau = 1/3$. In Fig. 6.1 we depict the density distribution for $K = 0.00001$

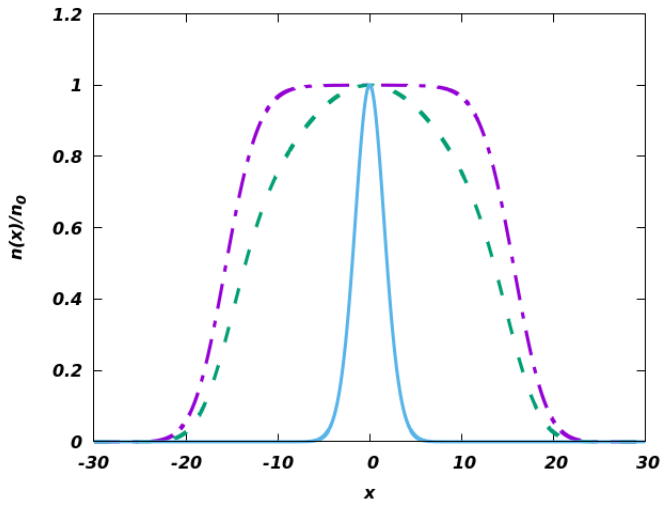

Figure 6.1: The density profile of the numerical solution for different K value is depicted here. The purple dashed-dotted line described the density for $K = 0.00001$, the green dashed line describes $K = 0.001$ and the blue solid line is prepared for $K = 0.1$. Here, $\tau = \mathcal{G}_2/|\mathcal{G}_1| = 0.1$ and $\mathcal{G}_1$ is set at 1.

(purple dashed-dotted line), $K = 0.001$ (green dashed line) and $K = 0.1$ (blue solid line), respectively. We can clearly see that the density profile indicate towards a transition from a droplet to a soliton as the trap frequency is increased. At very low trap frequency, that is $K = 0.00001$, the density plateau is distinctly visible indicating the droplet state. However, with gradual increase in trap frequency (say at $K = 0.001$) we observe a bell like structure. A tighter confinement leads to the generation of bright soliton as described by the solid blue line. The figure was obtained for $\tau = 0.1$ however, we note that the profile is not significantly altered for larger values of τ till $\tau = 0.9$. It is interesting to note that similar transition has already been observed for dipolar BEC where the dipolar interaction strength plays the analogous role of the trapping potential [98].

To excavate more on droplet-soliton transition, the chemical potential can be regarded as an important physical parameter. Hence, we assume, $\psi(x,t) = \phi(x)e^{-i\mu t}$ and apply in

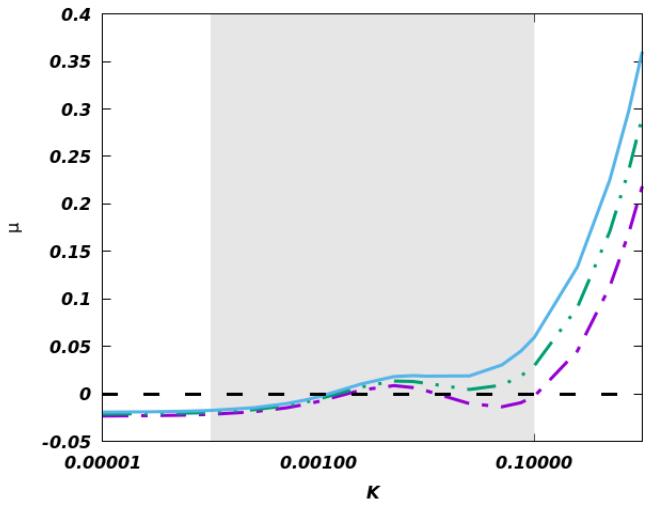

Figure 6.2: The variation of the chemical potential for different τ is noted here. The solid blue line corresponds to $\tau = 0.9$, green dashed-double-dotted line corresponds to $\tau = 0.5$ and purple dashed-dotted lines describe variation of the chemical potential with trap frequency for $\tau = 0.1$. $\mu = 0$ is marked with the black dashed line. The shaded area describes the region where we obtain a smooth transition from droplet to soliton.

Eq.(2.6). This results,

$$\mu\phi(x) = \left[-\frac{1}{2}\frac{d^2}{dx^2} + \frac{1}{2}Kx^2 + \mathcal{G}_1\phi^2(x) + \mathcal{G}_2\phi^3(x)\right]\phi(x). \tag{6.1}$$

Applying the normalization condition $\int_{-\infty}^{\infty}\phi^2(x)dx = 1$ we obtain,

$$\mu = \int_{-\infty}^{\infty}\left[\frac{1}{2}\left(\frac{d\phi}{dx}\right)^2 + \phi^2(x)\left(\frac{1}{2}Kx^2 + \mathcal{G}_1\phi^2(x) + \mathcal{G}_2\phi^3(x)\right)\right]dx. \tag{6.2}$$

We report the variation of the chemical potential with trap frequency for different BMF interaction strength in Fig. 6.2. The purple dashed-dotted line, green dashed-double-dotted line and blue solid line depicts $\tau = 0.1, 0.5$ and 0.9, respectively. For weaker trap frequency the system moves more in the droplet region which is signified by the negative

value of the chemical potential. A very weak trap frequency also leads the system to a nearly homogeneous setup where we obtain the chemical potentials for different τ is converging to ~ -0.02. Interestingly, similar result we have already reported for $\tau = 0.33$ [60]. As noted in Fig. 6.1, the stronger confinement leads to the solitonic state with $\mu > 0$ (right side of the grey shaded region of Fig. 6.2). However, we observe a non-monotonic behaviour in the region $K = 0.001$ and 0.1 in the figure (the grey shaded region). A comparison with Fig. 6.1 encourages us to consider this frequency window as the transition region as we observe a bell-like density profile for $K = 0.001$.

To investigate the transition, we then calculate the first derivative of chemical potential with respect to the trap frequency. The obtained result is depicted in Fig. 6.3. The main question here, is whether the transition is a phase transition (quantum) or a crossover. We know that, for quantum phase transition (QPT) we observe sudden variation in the ground state of the many body system when a controlling parameter (λ) of the Hamiltonian crosses a critical value [99, 100]. Here, we recognize $\lambda = K$, or the longitudinal trapping frequency. However, in Fig. 6.2 and Fig. 6.3 we do not observe any abrupt change in the chemical potential. Thus, to our assessment the transition appears to be gradual and hence can be termed as a crossover. Based on these evidence we can also quantify the crossover region as $0.0001 \lesssim K \lesssim 0.1$ (described in the grey shaded region in the figures).

Further, we calculate the total energy which can be defined as,

$$E = \int_{-\infty}^{\infty} \left[\frac{1}{2} \left(\frac{d\phi}{dx} \right)^2 + \phi^2(x) \left(\frac{1}{2} K x^2 + \frac{1}{2} \mathcal{G}_1 \phi^2(x) + \frac{2}{5} \mathcal{G}_2 \phi^3(x) \right) \right] dx. \quad (6.3)$$

The variation of energy corresponding to the trap frequency modulation is captured in Fig. 6.4. The figure reveals that the energy is negative for weak confinement suggesting the accumulation of droplet-like bound pairs. The energy crosses the zero line in the vicinity of $K = 0.001$ indicating the breakdown of droplet-like bound pairs. However, the energy flattening in the shaded area might be suggestive of an equilibrium of dropleton-soliton mixture. The bell-shaped density profile can be noted as a signature of mixed type of states. Further tightening of the longitudinal frequency leads to the total destruction of the

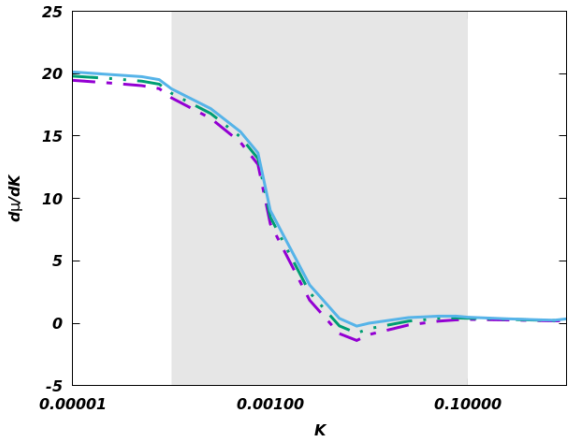

Figure 6.3: The first derivative of chemical potential w.r.t the trap frequency at different τ is described. The color coding and the line types for three different τ follows the same definition as of Fig. 6.2. The shaded region describes the transition.

droplets.

Next, we calculate the root-mean-square (rms) ($\sqrt{\langle x^2 \rangle}$) size of the condensate to study the size variation in the droplet-soliton transition as depicted in Fig. 6.5. The rms size is depicted in units of the rms size ($\sqrt{\langle x_0^2 \rangle}$) for $K = 0$. The figure clearly reflects on the fact that the variation of the BMF interaction does not have much contribution on the droplet size of the condensate as we report the variation for $\tau = 0.1$ (solid red line), 0.5 (solid green squares) and 0.9 (solid blue circles), respectively. We can also conclude that the weak confinement allows the larger pair size (with asymptotic limit extending to 1) suggesting the droplet formation and gradually the pair size smoothly falls off as we increase the longitudinal frequency. We also observe that the pair size drops much faster in the shaded region, which we have defined as the crossover region. The rms curve flattens thereafter and asymptotically reaches $1/10$ of the droplet size for a tightly confined 1D geometry. The effect of the variation in τ is apparently negligible for the normalized pair size, as noted in the figure.

It is also instructive now to investigate the role of particle number of the condensate.

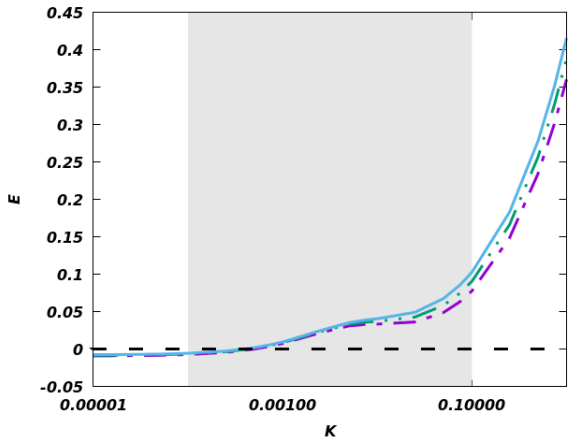

Figure 6.4: Change in energy with variation in the trap frequency is plotted here for different BMF interaction strengths. Again, the solid blue line, green dashed-double-dotted and purple dashed-dotted line denotes the energy variation as a function of trap frequency for $\tau = 0.9, 0.5$ and 0.1, respectively. $E = 0$ is marked by the black dashed line. The grey area corresponds to the region of transition from droplet to soliton.

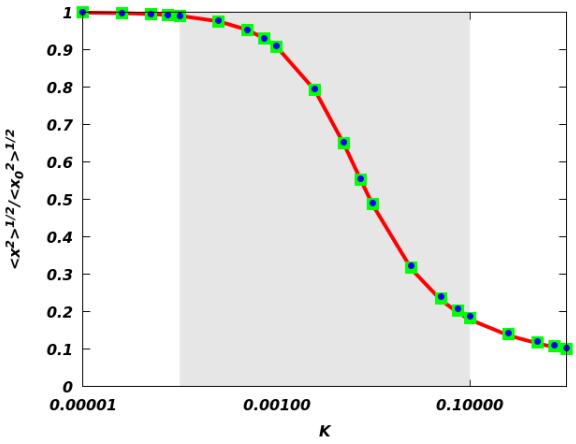

Figure 6.5: The figure describes the variation of the rms size of the droplets with the modulation of the trapping potential. The rms size is defined in units of $\sqrt{\langle x_0^2 \rangle}$ where $\langle x_0^2 \rangle$ is the rms size for $K = 0$. The solid red line presents $\tau = 0.1$, the green solid squares are for $\tau = 0.5$ and the blue solid circles denotes $\tau = 0.9$. The shaded portion describes the crossover area.

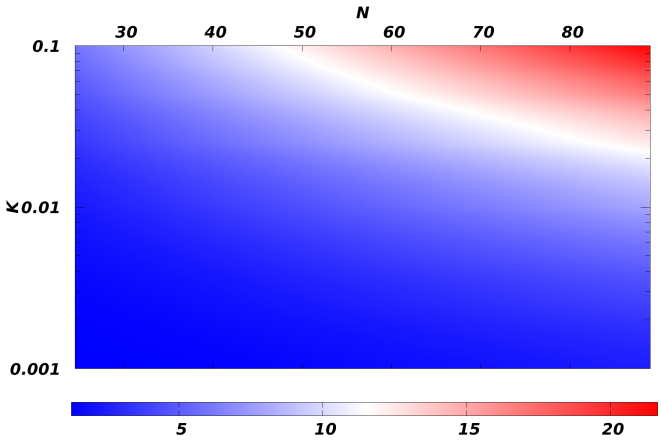

Figure 6.6: The figure describes the variation of the peak density as a function of particle number and K for $\tau = 0.1$. A progressive phase separation can be noted.

It must be noted that peak density is a good indicator in understanding the droplet and the solitonic states as it does not change for droplets, whereas noticeable change can be viewed for a soliton. We draw a phase diagram for the peak density as a function of the longitudinal harmonic confinement and the particle number as depicted in Fig. 6.6. The extended blue region suggests of nearly constant peak density, thereby pointing towards the existence of droplet-like states. A relatively tighter confinement in the realm of Q1D geometry, we observe progressive changes in the peak density which suggests of an emergence of localized soliton-like states.

For further clarity we report the peak density n_0 for different trap potential in Fig. 6.7. At weak trapping potential the density remains constant, thereby indicating the incompressible liquid-like state while progressive increase in the potential leads to the variation of the peak density suggesting higher compressibility which can be noted as a signature of gaseous soliton-like phase. The nature remains unchanged for different particle number as well as various values of τ values.

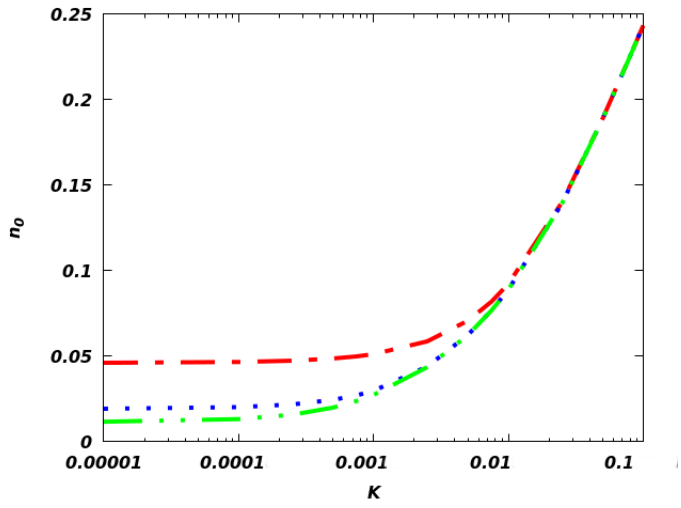

Figure 6.7: The figure describes the variation of the peak density (n_0) while the trapping potential is changed. The red dashed-dotted line describes $N = 25$ while variation of n_0 for $N = 50$ is depicted via blue dotted line. The green dashed-double-dotted line represents $N = 80$. The plot is prepared for $\tau = 0.1$.

6.2 Concluding Remarks

Here, we start from where we left in the previous analytical description and explore the droplet state numerically in inhomogeneous Q1D system. We find that the longitudinal trap frequency can be an appropriate controlling parameter in experiments to access a crossover from a droplet to a solitonic mode. We observe, that at very weak trap frequencies, the droplet states do exist just like as they do in the homogeneous case. However, with systematic increase in the trapping potential we move from flat top droplet solution to bell shaped solution and later to the emergence of solitons. In this regard, we especially emphasize on the numerical calculation of the chemical potential and energy. For very weak trapping potential, the chemical potential converges to the analytical value reported earlier [60]. At moderate values of the trapping frequency, the behavior of μ is nonlinear (the shaded regions in figure) and we observe a plateau in energy. Here, the droplet and soliton appear to be coexisting, corresponding to a bell type structure in the density. At relatively tighter

confinement, the bound droplets completely disappear and the solitonic mode prevails. We have repeated our investigation for different BMF interactions strengths ($\tau = 0.1, 0.5$ and 0.9) while noting a similar trend in the transition. To characterize the transition, we calculate the derivative of chemical potential however, we do not observe any significant change in the derivative as a function of the change of the Hamiltonian parameter (K here). We also observe a smooth transition of the pair size across a weak to a strong confinement domain. This allows us to conclude that the droplet to soliton transition denotes a crossover phenomenon.

Chapter 7

Conclusions And Future Outlook

We have presented the theoretical prescriptions to examine the newly observed liquid like state in ultra-cold atomic gases. To be precise, we have confined ourselves to Q1D it is widely used in experiments to create a condensate and study its dynamics.

We study the Q1D geometry and analyze the analytically obtained solution for a CQNLSE. We first explore the possibility of obtaining cnoidal solution for a generic CQNLSE and for that we observe the necessity of cnoidal trapping potential. Then we move our analysis towards optical trapping. Our main intention was to replicate supersolid-like behavior without using spin-orbit coupling or dipolar interaction. We took BOL for trapping in a DCQNLSE and obtained static solution. Through dynamical analysis the obtained stripes point to the supersolid phase. Moreover, we look into the superfluid-insulator dynamical phase transition and study the supercurrent. The spatio-temporal variation of supercurrent closely resembles to the behaviour of the stripes. The energy variation as a function of time demonstrates rapid nonlinear compression, which in turn mimics the occurrence of resonances in this system.

We present the analytical solution for droplets in a homogeneous CQNLSE and then we study the effect of harmonic trapping. It comes out that, trap modulation can even induce a droplet to soliton transition. As we report a confinement driven transition from droplet to soliton, we expect to open up new avenues in understanding the droplet state. We believe a study of fidelity of the numerically obtained solutions can shed more light in understanding

the transition [99].

The similarity between classical liquid and quantum droplet is that both are incompressible in nature. Quantum droplet is still a gas, but it stays bound for a longer time that a BEC gas without a trap. In our theoretical formulation we have not considered the three-body loss during droplet formation. The lifetime of droplet can be estimated including the three-body loss term. Droplets can undergo self-evaporation to stay stable. But the effect of three-body loss with increasing number of particles and rise of temperature from $T = 0$ restricts it's lifetime.

Solitons are bound state similar to droplets except their stabilization process is different. We can distinct soliton from droplet by analysing their collisional property as former one does not alter it's shape upon collision but latter one behaves differently depending on their momentum, particle number and phase. The dynamical analysis of the droplets in different environment can reveal interesting physics. Quantum reflection is a very interesting property which is shown by solitons in presence of a well [101]. Similar kind of behavior can be studied in case of droplets. Droplets are created because of a fine balance between the nonlinearities. The effect of kinetic energy is very small. As we have studied the effect of different nonlinearity ratios on droplets, it will be interesting to see their behavior under scattering with a defect.

Since, this area of research is still at its infancy thus we expect our effort in the recent theoretical developments on the liquid-like state will be subject of interest for a wide audience.

References

[1] Dmitry S Petrov. Liquid beyond the van der waals paradigm. *Nature Physics*, 14(3):211–212, 2018.

[2] Christopher J Pethick and Henrik Smith. *Bose–Einstein condensation in dilute gases*. Cambridge university press, 2008.

[3] Igor Ferrier-Barbut. Ultradilute quantum droplets. *Physics Today*, 72(4):46–52, 2019.

[4] D. S. Petrov. Quantum mechanical stabilization of a collapsing bose-bose mixture. *Phys. Rev. Lett.*, 115:155302, Oct 2015.

[5] CR Cabrera, L Tanzi, J Sanz, B Naylor, P Thomas, P Cheiney, and L Tarruell. Quantum liquid droplets in a mixture of bose-einstein condensates. *Science*, 359(6373):301–304, 2018.

[6] P. Cheiney, C. R. Cabrera, J. Sanz, B. Naylor, L. Tanzi, and L. Tarruell. Bright soliton to quantum droplet transition in a mixture of bose-einstein condensates. *Phys. Rev. Lett.*, 120:135301, Mar 2018.

[7] Giovanni Ferioli, Giulia Semeghini, Leonardo Masi, Giovanni Giusti, Giovanni Modugno, Massimo Inguscio, Albert Gallemí, Alessio Recati, and Marco Fattori. Collisions of self-bound quantum droplets. *Phys. Rev. Lett.*, 122:090401, Mar 2019.

[8] G. Semeghini, G. Ferioli, L. Masi, C. Mazzinghi, L. Wolswijk, F. Minardi, M. Modugno, G. Modugno, M. Inguscio, and M. Fattori. Self-bound quantum droplets of atomic mixtures in free space. *Phys. Rev. Lett.*, 120:235301, Jun 2018.

[9] G. Ferioli, G. Semeghini, S. Terradas-Briansó, L. Masi, M. Fattori, and M. Modugno. Dynamical formation of quantum droplets in a ^{39}K mixture. *Phys. Rev. Research*, 2:013269, Mar 2020.

[10] C. D'Errico, A. Burchianti, M. Prevedelli, L. Salasnich, F. Ancilotto, M. Modugno, F. Minardi, and C. Fort. Observation of quantum droplets in a heteronuclear bosonic mixture. *Phys. Rev. Research*, 1:033155, Dec 2019.

[11] Alessia Burchianti, Chiara D'Errico, Marco Prevedelli, Luca Salasnich, Francesco Ancilotto, Michele Modugno, Francesco Minardi, and Chiara Fort. A dual-species bose-einstein condensate with attractive interspecies interactions. *Condensed Matter*, 5(1):21, 2020.

[12] Zhichao Guo, Fan Jia, Lintao Li, and Dajun Wang. Quantum droplet in a mixture of rb and na bose-einstein condensates. In *APS Division of Atomic, Molecular and Optical Physics Meeting Abstracts*, volume 2020, pages E01–102, 2020.

[13] Holger Kadau, Matthias Schmitt, Matthias Wenzel, Clarissa Wink, Thomas Maier, Igor Ferrier-Barbut, and Tilman Pfau. Observing the rosensweig instability of a quantum ferrofluid. *Nature*, 530(7589):194, 2016.

[14] Igor Ferrier-Barbut, Holger Kadau, Matthias Schmitt, Matthias Wenzel, and Tilman Pfau. Observation of quantum droplets in a strongly dipolar bose gas. *Phys. Rev. Lett.*, 116:215301, May 2016.

[15] Igor Ferrier-Barbut, Matthias Schmitt, Matthias Wenzel, Holger Kadau, and Tilman Pfau. Liquid quantum droplets of ultracold magnetic atoms. *Journal of Physics B: Atomic, Molecular and Optical Physics*, 49(21):214004, 2016.

[16] Matthias Schmitt, Matthias Wenzel, Fabian Böttcher, Igor Ferrier-Barbut, and Tilman Pfau. Self-bound droplets of a dilute magnetic quantum liquid. *Nature*, 539(7628):259–262, 2016.

[17] Igor Ferrier-Barbut, Matthias Wenzel, Fabian Böttcher, Tim Langen, Mathieu Isoard, Sandro Stringari, and Tilman Pfau. Scissors mode of dipolar quantum droplets of dysprosium atoms. *Phys. Rev. Lett.*, 120:160402, Apr 2018.

[18] E Lucioni, L Tanzi, A Fregosi, J Catani, S Gozzini, M Inguscio, A Fioretti, C Gabbanini, and G Modugno. Dysprosium dipolar bose-einstein condensate with broad feshbach resonances. *Physical Review A*, 97(6):060701, 2018.

[19] L Chomaz, S Baier, D Petter, MJ Mark, F Wächtler, Luis Santos, and F Ferlaino. Quantum-fluctuation-driven crossover from a dilute bose-einstein condensate to a macrodroplet in a dipolar quantum fluid. *Physical Review X*, 6(4):041039, 2016.

[20] Eugene P Gross. Structure of a quantized vortex in boson systems. *Il Nuovo Cimento (1955-1965)*, 20(3):454–477, 1961.

[21] LP Pitaevskii. Vortex lines in an imperfect bose gas. *Sov. Phys. JETP*, 13(2):451–454, 1961.

[22] Franco Dalfovo, Stefano Giorgini, Lev P. Pitaevskii, and Sandro Stringari. Theory of bose-einstein condensation in trapped gases. *Rev. Mod. Phys.*, 71:463–512, Apr 1999.

[23] Stefano Giorgini, Lev P. Pitaevskii, and Sandro Stringari. Theory of ultracold atomic fermi gases. *Rev. Mod. Phys.*, 80:1215–1274, Oct 2008.

[24] Immanuel Bloch, Jean Dalibard, and Wilhelm Zwerger. Many-body physics with ultracold gases. *Rev. Mod. Phys.*, 80:885–964, Jul 2008.

[25] Alberto Cappellaro, Tommaso Macrì, and Luca Salasnich. Collective modes across the soliton-droplet crossover in binary bose mixtures. *Phys. Rev. A*, 97:053623, May 2018.

[26] Nils B Jørgensen, Georg M Bruun, and Jan J Arlt. Dilute fluid governed by quantum fluctuations. *Physical review letters*, 121(17):173403, 2018.

[27] T. D. Lee, Kerson Huang, and C. N. Yang. Eigenvalues and eigenfunctions of a bose system of hard spheres and its low-temperature properties. *Phys. Rev.*, 106:1135–1145, Jun 1957.

[28] Rajneesh Atre, Prasanta K Panigrahi, and Girish Saran Agarwal. Class of solitary wave solutions of the one-dimensional gross-pitaevskii equation. *Physical Review E*, 73(5):056611, 2006.

[29] Francesco Ancilotto, Manuel Barranco, Montserrat Guilleumas, and Martí Pi. Self-bound ultradilute bose mixtures within local density approximation. *Physical Review A*, 98(5):053623, 2018.

[30] EM Lifshitz and LP Pitaevskii. Statistical physics, part 2 (pergamon press, oxford. 1980.

[31] Joshua Soneson and Avner Peleg. Effect of quintic nonlinearity on soliton collisions in optical fibers. *Physica D: Nonlinear Phenomena*, 195(1-2):123–140, 2004.

[32] Belén Paredes, Artur Widera, Valentin Murg, Olaf Mandel, Simon Fölling, Ignacio Cirac, Gora V Shlyapnikov, Theodor W Hänsch, and Immanuel Bloch. Tonks–girardeau gas of ultracold atoms in an optical lattice. *Nature*, 429(6989):277–281, 2004.

[33] Aurel Bulgac. Dilute quantum droplets. *Phys. Rev. Lett.*, 89:050402, Jul 2002.

[34] Argha Debnath and Ayan Khan. On solving cubic-quartic nonlinear schrödinger equation in a cnoidal trap. *The European Physical Journal D*, 74(9):184, 2020.

[35] L Khaykovich, F Schreck, G Ferrari, Thomas Bourdel, Julien Cubizolles, Lincoln D Carr, Yvan Castin, and Christophe Salomon. Formation of a matter-wave bright soliton. *Science*, 296(5571):1290–1293, 2002.

[36] L. Salasnich, A. Parola, and L. Reatto. Effective wave equations for the dynamics of cigar-shaped and disk-shaped bose condensates. *Phys. Rev. A*, 65:043614, Apr 2002.

[37] Priyam Das, Ayan Khan, and Anirban Pathak. Formation of solitonic bound state via light-matter interaction. *The European Physical Journal D*, 74(10):1–8, 2020.

[38] D. S. Petrov and G. E. Astrakharchik. Ultradilute low-dimensional liquids. *Phys. Rev. Lett.*, 117:100401, Sep 2016.

[39] Katsuya Inui, Ben Nohara, Takuya Yamano, and Akio Arimoto. On solitons of standing wave solutions for the cubic-quartic nonlinear schrodinger equation (dynamics of functional equations and mathematical models). *RIMS Kokyuroku*, 1637:145, 04 2009.

[40] T Yamano. Phase portrait analysis for the envelope solution of cubic-quartic nonlinear schroedinger equations. *Hokkaido University Technical Report Series in Mathematics*, 140, 2009.

[41] Milton Abramowitz and Irene A Stegun. *Handbook of mathematical functions: with formulas, graphs, and mathematical tables*, volume 55. Courier Corporation, 1965.

[42] Shingo Takeuchi. Generalized jacobian elliptic functions and their application to bifurcation problems associated with p-laplacian. *Journal of Mathematical Analysis and Applications*, 385(1):24–35, 2012.

[43] Govind P Agrawal. *Fiber-optic communication systems*, volume 222. John Wiley & Sons, 2012.

[44] Utpal Roy, Rajneesh Atre, C Sudheesh, C Nagaraja Kumar, and Prasanta K Panigrahi. Complex solitons in bose–einstein condensates with two- and three-body interactions. *Journal of Physics B: Atomic, Molecular and Optical Physics*, 43(2):025003, jan 2010.

[45] Utpal Roy, B Shah, Kumar Abhinav, and P K Panigrahi. Gapped solitons and periodic excitations in strongly coupled BECs. *Journal of Physics B: Atomic, Molecular and Optical Physics*, 44(3):035302, jan 2011.

[46] Roger K Dodd, Hedley C Morris, JC Eilbeck, and JD Gibbon. Soliton and nonlinear wave equations. *nyap*, 1982.

[47] NG Vakhitov and Aleksandr A Kolokolov. Stationary solutions of the wave equation in a medium with nonlinearity saturation. *Radiophysics and Quantum Electronics*, 16(7):783–789, 1973.

[48] Priyam Das and Prasanta K Panigrahi. Controlled generation of nonlinear resonances through sinusoidal lattice modes in bose-einstein condensate. *Laser Physics*, 25(12):125501, 2015.

[49] Dmitry E. Pelinovsky, Vsevolod V. Afanasjev, and Yuri S. Kivshar. Nonlinear theory of oscillating, decaying, and collapsing solitons in the generalized nonlinear schrödinger equation. *Phys. Rev. E*, 53:1940–1953, Feb 1996.

[50] Hidetsugu Sakaguchi and Boris A. Malomed. Solitons in combined linear and nonlinear lattice potentials. *Phys. Rev. A*, 81:013624, Jan 2010.

[51] JA González, MA García-Nustes, Angel Sánchez, and Peter VE McClintock. Hawking-like emission in kink-soliton escape from a potential well. *New Journal of Physics*, 10(11):113015, 2008.

[52] Massimo Boninsegni and Nikolay V. Prokof'ev. Colloquium: Supersolids: What and where are they? *Rev. Mod. Phys.*, 84:759–776, May 2012.

[53] Jun-Ru Li, Jeongwon Lee, Wujie Huang, Sean Burchesky, Boris Shteynas, Furkan Çağrı Top, Alan O Jamison, and Wolfgang Ketterle. A stripe phase with supersolid properties in spin–orbit-coupled bose–einstein condensates. *Nature*, 543(7643):91–94, 2017.

[54] Tobias Donner. Dipolar quantum gases go supersolid. *Physics*, 12:38, 2019.

[55] Luca Tanzi, Eleonora Lucioni, Francesca Famà, Jacopo Catani, Andrea Fioretti, Carlo Gabbanini, Russell N Bisset, Luis Santos, and Giovanni Modugno. Observation of a dipolar quantum gas with metastable supersolid properties. *Physical review letters*, 122(13):130405, 2019.

[56] Fabian Böttcher, Jan-Niklas Schmidt, Matthias Wenzel, Jens Hertkorn, Mingyang Guo, Tim Langen, and Tilman Pfau. Transient supersolid properties in an array of dipolar quantum droplets. *Physical Review X*, 9(1):011051, 2019.

[57] L Chomaz, D Petter, P Ilzhöfer, G Natale, A Trautmann, C Politi, G Durastante, RMW Van Bijnen, A Patscheider, M Sohmen, et al. Long-lived and transient supersolid behaviors in dipolar quantum gases. *Physical Review X*, 9(2):021012, 2019.

[58] Vyacheslav I Yukalov. Saga of superfluid solids. *Physics*, 2(1):49–66, 2020.

[59] Maximilian Sohmen, Claudia Politi, Lauritz Klaus, Lauriane Chomaz, Manfred J. Mark, Matthew A. Norcia, and Francesca Ferlaino. Birth, life, and death of a dipolar supersolid. *Phys. Rev. Lett.*, 126:233401, Jun 2021.

[60] Argha Debnath and Ayan Khan. Investigation of quantum droplets: An analytical approach. *Annalen der Physik*, 533(3):2000549, 2021.

[61] Matthew Edmonds, Thomas Bland, and Nick G Parker. Quantum droplets of quasi-one-dimensional dipolar bose-einstein condensates. *arXiv preprint arXiv:2002.07958*, 2020.

[62] Mithilesh K Kumar Parit, Gargi Tyagi, Dheerendra Singh, and Prasanta K Panigrahi. Supersolid behavior in one-dimensional self-trapped bose-einstein condensate. *Journal of Physics B: Atomic, Molecular and Optical Physics*, 2021.

[63] GE Astrakharchik and Boris A Malomed. Dynamics of one-dimensional quantum droplets. *Physical Review A*, 98(1):013631, 2018.

[64] Nath Ajay, Bera Jayanta, Ghosh Suranjana, and Utpal Roy. Exact analytical model for bose-einstein condensate at negative temperature. *Scientific Reports (Nature Publisher Group)*, 10(1), 2020.

[65] Aleksandr Mikhailovich Lyapunov. The general problem of the stability of motion. *International journal of control*, 55(3):531–534, 1992.

[66] John AD Appleby, Xuerong Mao, and Alexandra Rodkina. Stabilization and destabilization of nonlinear differential equations by noise. *IEEE Transactions on Automatic Control*, 53(3):683–691, 2008.

[67] T Solomon Raju, C Nagaraja Kumar, and Prasanta K Panigrahi. On exact solitary wave solutions of the nonlinear schrödinger equation with a source. *Journal of Physics A: Mathematical and General*, 38(16):L271, 2005.

[68] Kevin E Strecker, Guthrie B Partridge, Andrew G Truscott, and Randall G Hulet. Formation and propagation of matter-wave soliton trains. *Nature*, 417(6885):150–153, 2002.

[69] Elliott H Lieb and Werner Liniger. Exact analysis of an interacting bose gas. i. the general solution and the ground state. *Physical Review*, 130(4):1605, 1963.

[70] Viktor Nikolaevich Popov. On the theory of the superfluidity of two-and one-dimensional bose systems. *Theoretical and mathematical physics*, 11(3):565–573, 1972.

[71] Tobias Ilg, Jan Kumlin, Luis Santos, Dmitry S Petrov, and Hans Peter Büchler. Dimensional crossover for the beyond-mean-field correction in bose gases. *Physical Review A*, 98(5):051604, 2018.

[72] D. Edler, C. Mishra, F. Wächtler, R. Nath, S. Sinha, and L. Santos. Quantum fluctuations in quasi-one-dimensional dipolar bose-einstein condensates. *Phys. Rev. Lett.*, 119:050403, Aug 2017.

[73] Tobias Paul, Klaus Richter, and Peter Schlagheck. Nonlinear resonant transport of bose-einstein condensates. *Phys. Rev. Lett.*, 94:020404, Jan 2005.

[74] Zhenya Yan, Xiao-Fei Zhang, and W. M. Liu. Nonautonomous matter waves in a waveguide. *Phys. Rev. A*, 84:023627, Aug 2011.

[75] Ritu Pal, Shally Loomba, Choragudi Nagaraja Kumar, Daniela Milovic, and Aleksandra Maluckov. Matter wave soliton solutions for driven gross–pitaevskii equation with distributed coefficients. *Annals of Physics*, 401:116–129, 2019.

[76] Wei Han, Gediminas Juzeliūnas, Wei Zhang, and Wu-Ming Liu. Supersolid with nontrivial topological spin textures in spin-orbit-coupled bose gases. *Physical Review A*, 91(1):013607, 2015.

[77] Cheng Chin, Rudolf Grimm, Paul Julienne, and Eite Tiesinga. Feshbach resonances in ultracold gases. *Rev. Mod. Phys.*, 82:1225–1286, Apr 2010.

[78] Maciej Lewenstein, Anna Sanpera, Veronica Ahufinger, Bogdan Damski, Aditi Sen, and Ujjwal Sen. Ultracold atomic gases in optical lattices: mimicking condensed matter physics and beyond. *Advances in Physics*, 56(2):243–379, 2007.

[79] Xiliang Zhang, Xiaoxi Xu, Yiyin Zheng, Zhaopin Chen, Bin Liu, Chunqing Huang, Boris A Malomed, and Yongyao Li. Semidiscrete quantum droplets and vortices. *Physical review letters*, 123(13):133901, 2019.

[80] Priyam Das. Lattice and quintic nonlinearity induced stripe phase in bose–einstein condensate under non-inertial and inertial motion. *Journal of Physics Communications*, 2(5):055012, 2018.

[81] Priyam Das, Ayan Khan, and Anirban Pathak. On the response of a bose-einstein condensate exposed to two counterpropagating ultra-fast laser beams. *arXiv preprint arXiv:1809.00171*, 2018.

[82] Ayan Khan and Prasanta K Panigrahi. Bell solitons in ultra-cold atomic fermi gas. *Journal of Physics B: Atomic, Molecular and Optical Physics*, 46(11):115302, 2013.

[83] Milton Abramowitz, Irene A Stegun, and Robert H Romer. Handbook of mathematical functions with formulas, graphs, and mathematical tables, 1988.

[84] A Smerzi, A Trombettoni, PG Kevrekidis, and AR Bishop. Dynamical superfluid-insulator transition in a chain of weakly coupled bose-einstein condensates. *Physical review letters*, 89(17):170402, 2002.

[85] FS Cataliotti, L Fallani, F Ferlaino, C Fort, P Maddaloni, and M Inguscio. Superfluid current disruption in a chain of weakly coupled bose–einstein condensates. *New Journal of Physics*, 5(1):71, 2003.

[86] Priyam Das, Manan Vyas, and Prasanta K Panigrahi. Loss of superfluidity in the bose–einstein condensate in an optical lattice with cubic and quintic nonlinearity. *Journal of Physics B: Atomic, Molecular and Optical Physics*, 42(24):245304, 2009.

[87] H Brezis and L Nirenberg. Positive solutions of nonlinear elliptic equations involving critical sobolev exponents. *Communications on Pure and Applied Mathematics*, XXXVI:437, 1983.

[88] Oliver Morsch and Markus Oberthaler. Dynamics of bose-einstein condensates in optical lattices. *Reviews of modern physics*, 78(1):179, 2006.

[89] Nicole Fabbri, David Clément, Leonardo Fallani, Chiara Fort, M Modugno, KMR Van Der Stam, and M Inguscio. Excitations of bose-einstein condensates in a one-dimensional periodic potential. *Physical Review A*, 79(4):043623, 2009.

[90] Elad Shamriz, Zhaopin Chen, and Boris A. Malomed. Suppression of the quasi-two-dimensional quantum collapse in the attraction field by the lee-huang-yang effect. *Phys. Rev. A*, 101:063628, Jun 2020.

[91] Thudiyangal Mithun, Aleksandra Maluckov, Kenichi Kasamatsu, Boris A Malomed, and Avinash Khare. Modulational instability, inter-component asymmetry, and formation of quantum droplets in one-dimensional binary bose gases. *Symmetry*, 12(1):174, 2020.

[92] Boris A. Malomed and Mark Ya. Azbel. Modulational instability of a wave scattered by a nonlinear center. *Phys. Rev. B*, 47:10402–10406, Apr 1993.

[93] Paulsamy Muruganandam and Sadhan K Adhikari. Fortran programs for the time-dependent gross–pitaevskii equation in a fully anisotropic trap. *Computer Physics Communications*, 180(10):1888–1912, 2009.

[94] Jason HV Nguyen, De Luo, and Randall G Hulet. Formation of matter-wave soliton trains by modulational instability. *Science*, 356(6336):422–426, 2017.

[95] Pierre-Gilles De Gennes. *Superconductivity of metals and alloys*. CRC Press, 2018.

[96] Poulumi Dey, Ayan Khan, Saurabh Basu, and B Tanatar. A comparison of harmonic confinement and disorder in inducing localization effects in a superconductor. In *International Journal of Modern Physics: Conference Series*, volume 11, pages 127–132. World Scientific, 2012.

[97] Boris A Malomed. The family of quantum droplets keeps expanding. *arXiv preprint arXiv:2010.13461*, 2020.

[98] Rafał Ołldziejewski, Wojciech Górecki, Krzysztof Pawłowski, and Kazimierz Rzażewski. Strongly correlated quantum droplets in quasi-1d dipolar bose gas. *Phys. Rev. Lett.*, 124:090401, Mar 2020.

[99] Ayan Khan and Pierbiagio Pieri. Ground-state fidelity in the bcs-bec crossover. *Phys. Rev. A*, 80:012303, Jul 2009.

[100] P Dey, D Sarkar, A Khan, and Saurabh Basu. Participation ratio and fidelity analyses as tools to study bcs-bec crossover. *The European Physical Journal B*, 81(1):95, 2011.

[101] Thomas Ernst and Joachim Brand. Resonant trapping in the transport of a matter-wave soliton through a quantum well. *Physical Review A*, 81(3):033614, 2010.

List of Publications

1. On Solving Cubic-Quartic Nonlinear Schrödinger Equation in a Cnoidal Trap, A. Debnath, A. Khan, Eur. Phys. J. D, 74, 184 (2020).

2. Investigation of Quantum Droplet: An Analytical Approach, A. Debnath and A. Khan, Ann. Phys., 533, 2000549 (2021).

3. Signature of Supersolidity in a Driven Cubic-Quartic Nonlinear Schrödinger Equation, A. Debnath, J. Tarun, A. Khan, Journal of Physics B: Atomic, Molecular and Optical Physics 55, 025301 (2022).

4. Dropleton-Soliton Crossover mediated via Trap Modulation, A. Debnath, A. Khan, S. Basu, Physics Letters A, 439, 128137 (2022).

5. Quantum Droplet In Lower Dimensions, A. Debnath, A. Khan, Frontiers in Physics. (In press)

BOOK CHAPTER

1. Jacobi Elliptic Functions and their Application in Ultra-cold Atomic Gases, A. Debnath and A. Khan, Springer Proceedings in Physics (SCOPUS) (ISSN: 0930-8989).